
Title: The effect of increasing V content on the structure, mechanical properties and oxidation resistance of Ti-Si-V-N films deposited by DC reactive magnetron sputtering

Author: F. Fernandes A. Loureiro T. Polcar A. Cavaleiro

PII: S0169-4332(13)01976-4
DOI: http://dx.doi.org/doi:10.1016/j.apsusc.2013.10.117
Reference: APSUSC 26581

To appear in: *APSUSC*

Received date: 26-6-2013
Revised date: 18-10-2013
Accepted date: 19-10-2013

Please cite this article as: F. Fernandes, A.L. </sup>,T. Polcar, A. Cavaleiro, The effect of increasing V content on the structure, mechanical properties and oxidation resistance of Ti-Si-V-N films deposited by DC reactive magnetron sputtering, *Applied Surface Science* (2013), http://dx.doi.org/10.1016/j.apsusc.2013.10.117

**Research Highlights**

- V is placed in solid solution in the fcc phase of low temperature deposited films.
- Regardless on V content, hardness and Young's modulus of TiSi(V)N films are similar
- Independently of Si content, V decreases the oxidation onset of films down to 500 $^{0}$C.
- Outwards diffusion of V and formation of $\alpha$-$V_2O_5$ oxide is the cause of low oxidation resistance.

# The effect of increasing V content on the structure, mechanical properties and oxidation resistance of Ti-Si-V-N films deposited by DC reactive magnetron sputtering

F. Fernandes[1*], A. Loureiro[1],T. Polcar[2,3], A. Cavaleiro[1]

[1]CEMUC - Department of Mechanical Engineering, University of Coimbra, Rua Luís Reis Santos, 3030-788 Coimbra, Portugal.

[2]Department of Control Engineering Czech Technical University in Prague Technicka 2, Prague 6, 166 27 Czech Republic.

[3]n-CATS University of Southampton Highfield Campus SO17 1BJ Southampton, UK.

[*]Email address: filipe.fernandes@dem.uc.pt, tel. + (351) 239 790 745, fax. + (351) 239 790 701

**Abstract**

In the last years, vanadium rich films have been introduced as possible candidates for self-lubrication at high temperatures, based on the formation of $V_2O_5$ oxide. The aim of this investigation was to study the effect of V additions on the structure, mechanical properties and oxidation resistance of Ti-Si-V-N coatings deposited by DC reactive magnetron sputtering. The results achieved for TiSiVN films were compared and discussed in relation to TiN and TiSiN films prepared as reference. All coatings presented a fcc NaCl-type structure. **A shift of the diffraction peaks to higher angles with increasing Si and V contents suggested the formation of a substitutional solid solution in TiN phase**. Hardness and Young's modulus of the coatings were similar regardless on V content. **The onset of oxidation of the films decreased significantly**

**to 500 °C when V was added into the films; this behaviour was independent of the Si and V contents.** The thermogravimetric isothermal curves of TiSiVN coatings oxidized at temperatures below the melting point of α-$V_2O_5$ (~685 °C) showed two stages: at an early stage, the weight increase over time is linear, whilst, in the second stage, a parabolic evolution can be fitted to the experimental data. At higher temperatures only a parabolic evolution was fitted. α-$V_2O_5$ was the main phase detected at the oxidized surface of the coatings. Reduction of α-$V_2O_5$ to β-$V_2O_5$ phase occurred for temperatures above its melting point.

Keywords: TiSi(V)N films, Structure, Mechanical properties, Oxidation resistance, Vanadium oxide

## 1 Introduction

High-speed cutting and dry machining processes without the use of environmental harmful lubrication requires milling tools capable to withstand severe conditions of wear, friction, oxidation and corrosion [1, 2]. Solid lubricants coatings, such as WC/C, $MoS_2$, diamond-like carbon (DLC), hex-BN as well as their combinations in nanocrystaline or multilayer structures, have been successfully applied in such parts in order to increase their lifetime and performance for various tribological applications. However, considerable degradation of the tribological effectiveness of these coatings at elevated temperature has been reported due to their low resistance to oxidation [3-5]. To overcome this shortcoming, a new concept of lubrication based on the formation of lubricious oxides has been proposed. This is the case of the so-called Magnéli oxide phases based on Ti, Si, Mo, W and V, which have easy shear able

planes [3, 6]. Among these elements, particular attention has been given to the vanadium-containing coatings (Magnéli phases $V_nO_{3n-1}$), which showed interesting tribological properties in the temperature range 500-700 $^0$C [3, 7-12]. **Dissimilar series of V-based hard coatings have been developed, such as ternary CrVN [13], (V,Ti)N [14], multilayer AlN/VN [15] and quaternary single layer or multilayered CrAlVN [16, 17] and TiAlVN [2, 8, 18, 19].** However, since other ternary coatings systems, based on (TiX)N with X = B, Cr, Al, Si, Cr, etc, have been attractive for advanced hard coating materials, the effect of vanadium doping to these systems should also be considered.

Among those ternary systems, most of the research works have been focused on TiSiN coatings deposited by CVD and/or PVD techniques [20, 21]. Depending on the deposition conditions, these coatings could be deposited with a nanocomposite structure, consisting of nano-sized TiN crystallites surrounded by an amorphous matrix of $Si_3N_4$ displaying very high hardness values [22], compared to any other ternary (TiX)N compound, with extremely good oxidation resistance [23, 24]. In other deposition conditions, substitutional solid solution of Si in TiN structure (not predicted by the Ti-Si-N phase diagram) could be achieved [22, 25, 26]. Relatively to the friction coefficient of Ti-Si-N coatings, the studies have reported values in the range [0.6 - 1.3] at room and high temperatures [27-29]. Since the addition of V successfully decreased the friction coefficient of binary and ternary systems (down to reported values of 0.2-0.3 at temperatures between 550-700 $^0$C), similar studies on the effect of V-addition should be performed on TiSiN coatings exhibiting unique mechanical properties and oxidation resistance.

This paper reports the first results on the effect of increasing vanadium content to Ti-Si-V-N films deposited by DC reactive magnetron sputtering. It is focused on

coating structure, mechanical properties and oxidation resistance. Comparison of the results with those achieved for reference TiN and TiSiN coatings is presented. The results of this study will support further research aimed at the tribological behavior of the coatings at high temperatures.

## 2 Experimental Procedure

**Three series of TiSiN films with different Si contents, each series with increasing V contents (TiSiVN coatings), were** deposited in a d.c. reactive magnetron sputtering machine equipped with two rectangular (100×200 mm) magnetron cathodes working in unbalanced mode. A high purity Ti (99.9%) target, with 18 holes of 10 mm in diameter (uniformly distributed throughout the preferential erosion zone of the target), and a high purity $TiSi_2$ (99.9%) composite target were used in the depositions. The different silicon contents were achieved by changing the power density applied to each target. The V content was varied by changing the number of high purity rods of Ti and V (with 10 mm in diameter) placed in the holes of the Ti target. 4, 8 and 12 cylindrical pieces of vanadium were used. In all the cases the total power applied to the targets was set to 1500 W. To serve as reference, a stoichiometric TiN coating was deposited from the Ti target. Hereinafter the coatings will be designated as Sx-y, where x is related to the specific power applied to the $TiSi_2$ target (see Table 1**), and therefore associated to the Si content on the coatings,** and y the number of V rods used in the depositions**, giving an indication of V content in each series of TiSiVN films**. **Thus, denomination S2-0, S2-4, S2-8 and S2-12 represents coatings from the same series, i.e. with identical Si content ($TiSi_2$ target power 1.5 W/cm$^2$), with**

**increasing V content from 0 up to a maximum content achieved for the coating produced using 12 vanadium pellets embedded into the Ti target.**

Polished high-speed steel (AISI M2) (Ø 20 x 3 mm, for mechanical properties measurements), FeCrAl alloy and alumina substrates (10 x 10 x 1 mm, for oxidation tests and structural analysis), stainless steel discs (Ø 20 × 1 mm, for residual stress measurements) and (111) silicon samples (10 x 10 x 0.8 mm, for thickness measurements and chemical composition evaluation) were used as substrates. Prior to the depositions, all the substrates were ultrasonically cleaned in acetone for 15 min and alcohol for 10 min. The substrates were mounted in a substrate holder (which revolved with 18 rev/min around the center axis) giving a target to substrate distance of 175 mm. Prior to deposition, the chamber was evacuated down to $8.7 \times 10^{-4}$ Pa and the substrates were etched with Ar ion sputtering during 1h with a bias voltage of -650 V to remove any surface contaminants. In order to enhance the adhesion of the coatings, Ti and TiN adhesion layers of approximately 0.24 and 0.45 µm, respectively, were deposited on the substrates before TiSi(V)N coatings. In all the depositions, the total working gas pressure was kept constant at 0.3 Pa, using approximately 30 sccm of Ar and 17 sccm of $N_2$. The depositions were performed with a negative substrate bias of 50 V. The deposition time was set in order to obtain films with approximately 2.5 µm of total thickness (including interlayers). The deposition parameters are shown in Table 1.

The chemical composition of the coatings was evaluated by electron probe microanalysis (EPMA - Cameca SX 50). Crystallographic structure was investigated by X-ray diffraction (X' Pert Pro MPD diffractometer) using a grazing incidence angle of $1^0$ and Cu $K_{\alpha 1}$ radiation ($\lambda$ = 1.54060 Å). The XRD spectra were fitted by using a **pseudo-Voigt** function to calculate either the full width at half maximum (FWHM)

and the peak position (2□). The fracture cross-section morphology and the thickness of the films were investigated by scanning electron microscopy (SEM). Further, profilometer was used to confirm coating thickness and to evaluate surface roughness.

The hardness and Young's modulus of films were measured in a nano-indentation equipment (Micro Materials NanoTest) using a Berkovich diamond pyramid indenter. In order to avoid the effect of the substrate, the applied load (10 mN) was selected to keep the indentation depth less than 10% of the coating´s thickness. 32 measurements were performed in each sample. The level of residual stresses was calculated through the Stoney equation [30] by measuring the bulk deflection of the film-substrate body.

The oxidation resistance of the coatings was evaluated by thermogravimetric analysis (TGA) using industrial air (99.99% purity). The films deposited on alumina substrates were firstly heated with a constant temperature ramp of 20 $^0$C/min from room temperature up to 1200 $^0$C, in order to determine the onset point of oxidation. Then, coated specimens of FeCrAl alloy were subjected to isothermal tests at different selected temperatures and time. The weight gain of the samples was evaluated at regular 2 s intervals using a microbalance with an accuracy of 0.01 mg. The air flux used was 50 ml/min and the heating rate up to the isothermal temperature was 20 $^0$C/min. After oxidation tests, the surface morphology of the specimens was examined by scanning electron microscopy with energy dispersive x-ray spectroscopy (SEM-EDS) and their structure was evaluated by XRD diffraction. The oxide products on the surface were characterized by Raman spectroscopy.

## 3 Results and Discussion

### 3.1 Coatings Characterization

#### 3.1.1 Chemical composition and microstructure

The elemental chemical composition of the coatings determined by EPMA is shown in Table 2. As could be expected, the simultaneous decrease in the power density of Ti target and increase in the power density of $TiSi_2$ target gave rise to higher Si content in the coatings. Only insignificant variations were detected on the Si / Ti ratios with incorporation of V in the Ti target. **The nitrogen content of the coatings was close to 50 at.% regardless of Si and V.**

The corresponding X-ray diffraction patterns of the as-deposited coatings are displayed in Figure 1. **The influence of increasing V content on TiSiN coatings is shown in Figure 1 b) for the film with lower Si content, as representative of all series containing vanadium.** In all graphs TiN film pattern is shown as a reference. In all cases, the diffraction peaks could be generally assigned to the fcc NaCl-type crystalline TiN phase. The XRD pattern of the TiN reference coating reveals that all peaks are shifted to lower diffraction angles in relation to the standard ICDD card of TiN, probably indicating residual compressive stresses [31]. For TiSiN coatings with 3.8 and 6.7 at.% of Si, (200) peak vanishes and the sharpening of the peaks suggests larger grain size. Based on Scherrer´s equation, grain sizes of 16 nm and 24 nm were calculated for TiN and coatings with low Si content, respectively. With further increase of the Si content (12.6 at.% of Si) a strong decrease of the peaks intensity, as well as their significant broadening (a grain size of 6 nm was calculated), are observed

suggesting a decrease of crystallinity. With increasing Si content, the fcc peaks are shifted to higher angles, behaviour associated to a smaller unit cell. This can be explained by the presence of Si in solid solution, since its smaller atomic radius promotes the contraction of the TiN lattice. Therefore, in this case the stoichiometric phases (TiN + $Si_3N_4$) do not segregate and nanocomposite structure is not formed. Such behaviour could be explained by the low deposition temperature together with low substrate ion bombardment, which do not provide the necessary mobility of the species for the nanocomposite formation [22]. This observation is in agreement with the results from the literature, where similar solid solutions and changes in the film orientation have been observed with silicon incorporation [21, 25, 32].

The coatings with V display similar XRD patterns and peaks to TiSiN. No significant changes in the peaks intensities or widths were observed, except for the highest Si content films where a small improvement in the crystallinity was detected. All the vanadium containing films had the XRD peaks shifted to higher angles, behaviour, once again, related to a smaller unit cell due to the substitution of Ti by the smaller V atoms. Similar trend was observed by Pfeiler et al [2] for the TiAlVN system.

Figure 2 displays typical surface and fracture cross section-micrographs of TiSiVN coatings. All coatings showed a typical columnar structure. As Si content was increased (see Figure 2 b) for coating S1-0), the columns size and the surface roughness were firstly reduced, for silicon contents of 3.8 and 6.7 at.%, and then increased for the highest silicon content, which is an opposite trend than that observed for the grain size. The addition of V did not change the global type of columnar morphology and the coating cross-section was similar. The only exception was the

strong increase of the size of the columns as well as the surface roughness (see Figure 2 c) for coating S1-12) for low silicon content coatings.

3.1.2 Hardness, Young's modulus and residual stresses

The dependence of the hardness and Young´s modulus on the Si and V content is shown in Figure 3. As the silicon content in the TiSiN films increases, the hardness of coatings reached a maximum value of 27 GPa at a Si content of 6.7 at.%; then it dropped with further increasing Si content to a lower value than the reference TiN. Although the grain grow is observed with increasing Si additions up to 6.7 at.% of Si, the hardening of coatings is mostly result of the nitride lattice distortion, which improves the resistance to plastic deformation (solid solution hardening). Residual stresses should not be a factor of hardness differentiation between the coatings, since all films have approximately the same level of compressive residual stresses, with any Si addition (~ 3 GPa). This result also supports what was stated above that the shift of the peaks to the right with Si additions is exclusively due to substitutional solid solution. The decrease in hardness with further Si addition is due to the loss of crystallinity associated with the lower degree of phase nitriding regardless on the lower grain size [26]. Young's modulus progressively decreases with increasing Si content, which is related to changes in the binding energy between ions due to Si incorporations. Similar hardness and Young's modulus evolution as a function of Si content has been reported in Refs [25, 33].

Concerning the effect of V addition on the hardness and Young´s modulus, similar evolution was observed for all films (see e.g. Figure 3 b) for S1-y films). Although the variations are very small and often within the error bars of the hardness

values, general trend is a slight increase in hardness followed by drop for the highest vanadium content. Coatings with the higher silicon content and with vanadium additions displayed lower hardness and Young's modulus values as compared to the other V rich coatings. The hardness enhance with V additions is probably due to the presence of V in solid solution. In fact, the similar level of residual stresses as function of V content measured, which revealed to be from the range of 3 – 4 GPa, and the observed shift of peaks to higher angles with V incorporation, supports the previous affirmation.

### 3.2 Continuous and Isothermal oxidation in air

The effect of increasing Si and V content on the onset point of oxidation of the TiN and TiSiN systems, respectively, are shown in Figure 4. Silicon incorporation strongly improved the onset of oxidation of the coatings, with the highest silicon content (S3-0) showing the highest oxidation resistance. **Kacsich et al. [34, 35] reported that the high oxidation resistance of these coatings was due to the presence of a protective silicon-rich oxide layer. This layer acted as an efficient diffusion barrier against oxygen and metal ions diffusion; thus, it protected the coating from further oxidation**. Our results showed that the onset point of oxidation of films decreased significantly down to a temperature of approximately 500 $^{0}$C (lower than TiN) for all coatings containing vanadium. Interestingly, this behaviour was independent of Si content of the films **and, therefore, the vanadium incorporation interfered with the diffusion of silicon and the consequent formation of a continuous protective silicon oxide layer.** Furthermore, all V-containing coatings were completely oxidized at a lower temperature than TiN film. Lewis et al. [7], Zhou et al.

[36], and Franz et al. [37], who studied the effect of V doping on the oxidation behavior of multilayered TiAlN/VN and CrAlVN coatings, respectively, also observed a similar decrease in the onset point of oxidation. In order to better characterize the oxidation behaviour of the V rich coatings, isothermal oxidation tests were conducted at selected temperatures using S2-8 coating deposited onto FeCrAl alloy substrates. The isothermal curves were compared with those of TiSiN coating with similar Si content and with TiN (see Figure 5).

Comparing the mass gain of the coatings and taking into account the testing temperature in each case, it is possible to conclude that V-free TiSiN coating (S2-0 tested at 900 $^0$C) is much more resistant to oxidation. This coating exhibits a typical parabolic oxidation weight gain as a function of time indicating the formation of protective silicon-rich oxide layer, as referred to above. Similar type of evolution is exhibited by TiN coating; however, in this case the titanium oxide scale does not protect the coatings and, thus, it is effective only at low isothermal temperature [38]. It should be remarked that during continuous oxidation test up to 1200 ºC, at 900 ºC TiN coatings was already half consumed. Regarding the isothermal curves of TiSiN coating with V additions (S2-8), it can be concluded that, independently of the isothermal temperature and time of exposure, their mass gain is always much higher than TiN and V-free TiSiN coatings (S2-0). The isothermal curves tested at 550 and 600 $^0$C showed two steps: at an early stage, the weight gain is rapidly increasing almost linearly up to approximately 0.1 mg/cm$^2$ (particularly at 600 $^0$C), whereas in the second stage, a parabolic evolution can be fitted. Isothermal annealing of S2-8 at 700 $^0$C shows significant increase of mass gain following the parabolic evolution.

### 3.2.1 Surface structure

As it would be expected, both TiN annealed at 600 $^0$C and S2-0 coating annealed at 900 $^0$C **exhibited several intense peaks belonging to the (110), (101), (200), (111) and (210) of a tetragonal phase related to rutile/$TiO_2$ (ICDD card 76-0649) (not shown here). Weak peaks assigned to TiN (ICDD card 87-0628) were observed in the XRD spectra of the S2-0 coating, which was in a good agreement with its annealing curve, since only partial oxidation of the film was expected. Moreover, diffraction peaks associated with Si oxide were not detected on the oxidized surface of S2-0 film suggesting an amorphous character of the protective oxide layer. This result is in agreement with literature, where similar observation was reported [34, 35].**

XRD patterns of S2-8 oxidized coatings in isothermal tests are shown in Figure 6. The main phases detected by XRD were Ti-V-O and V-O oxides; however, depending on the isothermal temperature and time, different orientations and peaks assigned to V-O were perceived. After annealing at 550 $^0$C during 1 h, the following phases could be identified: Ti(V)$O_2$ (ICDD card 77-0332) and α-$V_2O_5$ (ICDD card 72-0433) with a preferred orientation following the (001) plane (peak at 20.3º), together with the f.c.c. nitride from the coating. The same phases were detected at 600 $^0$C during 10 min, however, α-$V_2O_5$ phase showed random orientation. Further increase in isothermal time (annealing at 600 $^0$C during 30 min) resulted in loss of TiN peaks and the orientation of the α-$V_2O_5$ phase is again following (001) plane. The absence of TiN peaks is in good agreement with the isothermal curve shown in Figure 5. Progressive oxidation is demonstrated in the intensity of (001) reflection after 30 min of annealing, where the amount of α-$V_2O_5$ is clearly higher. These changes in phase proportion and

orientation have already been observed by several authors during the oxidation of TiAlN/VN multilayer and TiAlVN single layered coatings [1, 7, 8, 36]. Increasing the heat treatment to 700 $^0$C, which is temperature higher than the melting point of α-$V_2O_5$ (~685 $^0$C [10, 36]), resulted in the random orientation of this phase; moreover, a sharp peak at $2\theta = 12.8^0$ identified as β-$V_2O_5$ (ICDD card 45-1074) with (002) preferential orientation appearing [39]. β-$V_2O_5$ phase is a result of loss of O from α-$V_2O_5$, due to a reduction process [40]. **We should emphasize here that vanadium oxides observed on the oxidized surface are optimal from the tribological point of view. Vanadium oxide could acts as low-friction solid lubricant or, for higher temperatures, as liquid lubricant. Therefore the drop in onset oxidation temperature should not be considered as a significant drawback of TiSiVN coatings.**

### 3.2.2 Surface morphology and characterization

Typical SEM surface micrographs of the S2-0 and V-rich coating (S2-8) isothermally oxidized at different temperatures and times are shown in Figure 7 and 8, **respectively. EDS and Raman analyses were carried out on the oxidized surface of the coatings to identify their composition.** On the oxidized surface of the S2-0 film, two different zones could be detected**, a dark grey phase evenly distributed throughout the surface and white islands. EDS analysis showed that the white oxide was rich in Ti (crystals of $TiO_2$), and the dark grey phase composed mainly by Si and Ti**. The Raman spectra of these zones are plotted in Figure 9. As can be observed the light grey phase displays Raman active modes at 152, 253, 454 and 610 cm-1 [3, 23] assigned to rutile, confirming its presence in the oxidized coating detected by XRD. The same phase, with much less intensity, was detected for the dark grey

phase; however, strong additional peaks assigned to anatase ($TiO_2$) were observed. This finding corroborates the report of Pilloud et al. [23], who showed that anatase Raman bands increased with the silicon content in TiSiN films, whereas that of rutile decreased. As only strong peaks of rutile were detected by XRD, this indicates that the amount of anatase should be small and, therefore, not detectable by XRD diffraction. **Since Raman penetration depth is relatively limited, the absence of silicon oxide in Raman spectra indicated that Si-O was below the$TiO_2$ phase identified by XRD. This finding corroborates the results of Kacsich et al. [34, 35]; they observed titanium oxide layer formed at outmost surface and silicon oxide sublayer (TiSiN coatings).**

**The analysis of the oxidized surface of S2-8 coating reveals that the surface oxide morphology is different from that of coating S2-0. It displays** a floret-like structure formed by light and dark grey zones. At 550 ºC these phases are tiny distributed throughout the surface, being difficult to clearly identify the boundaries between them. At a temperature of 600 $^0$C, the separation between both zones is evident with the shape of darker zone suggesting some type of dendritic growth. With the increase of the isothermal time, an increase in the area covered by the grey dark phase was observed. The temperature 700 $^0$C led to a different oxide morphology, i.e. the appearance of a black zone in some rosettes and the segregation of a white phase to the boundaries of the floret-like structure. This change in the microstructure can be associated to the melting of $\alpha$-$V_2O_5$, which originates a smoother surface (Figure 8 d)). **Figure 10 shows examples of EDS spectra of points identified in Figure 8 (phases 1 and 2). As can be observed, Ti Kβ peak (4.931 keV) overlaps the V Kα peak (4.952 keV) and, therefore, V Kβ peak should be taken in consideration for analyzing V importance. In order to identify the different oxide phases marked in Figure 8, the**

**ratio between the peaks intensities of V Kβ (Si Kα) and Ti Kα from EDS analyses are summarized in Table 3. To a relative increase in this ratio corresponds the preferential formation of the oxide of that element.** EDS analyses of points 1 and 2 reveal similar compositions for the grey light and dark zones, suggesting the presence of oxides containing Ti, Si and V**. However, darker phase has clearly a higher V content (see Table 3).** The Raman spectrum taken at grey dark phase (see Figure 11) shows the presence of intense peaks assigned to α-$V_2O_5$ [3, 8, 10] and small peaks related to rutile ($TiO_2$). On light grey phase the spectrum is much less defined, with broader bands. α-$V_2O_5$ peaks almost vanished whereas rutile bands are enhanced. Low crystallized Ti-O phases give very similar Raman spectra, which evolve, after annealing, either as anatase or rutile [41, 42] phases. In summary, the dark grey phase can be assigned mainly to α-$V_2O_5$, and small quantities of $TiO_2$, probably as a bilayer with α-$V_2O_5$ on the top and $TiO_2$ underneath, as suggested by EDS measurements**. In fact, the high ratio of V/Ti of point 3 marked in Figure 8, allows identifying a V-rich oxide, on the surrounding regions of the dark grey phase.** The light grey phase should be attributed to low crystallized Ti(V)$O_2$. These results agree to the XRD results acquired on the oxidized surface of the films where both $TiO_2$ and α-$V_2O_5$ phases were indexed. When the isothermal time was prolonged from 10 to 30 min at 600 ºC, the increase of the intensity of the α-$V_2O_5$ peak observed in the XRD patterns was is in a good agreement with a higher amount of grey dark phase observed on the oxidized surface morphology.

Similarly to S2-0 coating signals from Si-O oxide were neither detected by XRD nor by Raman spectroscopy. However, according to EDS analysis this oxide should be present. As these signals are coming from a sub-surface layer, an oxide layer

rich in Ti and Si should coexist with a global chemical composition similar to that of light grey phase.

From the three different morphological zones of sample annealed at 700 $^0$C for 10 min (Figure 8 d), EDS analysis showed that the two grey phases were mainly rich in vanadium and oxygen. **Signals of elements from the substrate were detected in the dark phase, particularly Al, which in conjunction with XRD results, allowed identifying it as β-$V_2O_5$.** In fact, it is well known, that the loss of O from α-$V_2O_5$, due to a reduction process, leads to its transformation in β-$V_2O_5$ [40, 43]. The presence of highly oxygen reactive elements, such as aluminum, in the substrate can reduce the molten α-$V_2O_5$, subtracting O and promoting the formation of β-$V_2O_5$. The Raman spectra of the dark and light grey phases plotted in Figure 12 show similar Raman patterns with peaks related to $V_2O_5$. Both α- and β-$V_2O_5$ display similar Raman spectra [44]. **The segregated white areas located at the boundaries of the grey phase (see ratio Si/Ti of point 5) were rich in Si and Ti, suggesting to be silicon and titanium oxides.**

A good correlation was found between the isothermal oxidation curve, XRD measurements and surface morphology of S2-8 coating. At temperatures below the melting point of α-$V_2O_5$, the isothermal oxidation curve starts with a linear increase in the mass gain and then changes to a parabolic law. The XRD spectra of specimen S2-8 oxidized during 10 min at 600 $^0$C, in the first stage of the oxidation process, revealed the presence of intense peaks of α-$V_2O_5$. Further increase in isothermal time to 30 min showed an increased amount of α-$V_2O_5$, as confirmed by the increase of the grey dark phase, above attributed to V-rich zones. XRD pattern for this sample also showed an increase in $TiO_2$ peaks intensity suggesting a thickening of the oxide scale. Therefore, the first linear part of the isothermal curve is due to the oxidation of both titanium and

vanadium to form Ti(V)$O_2$ and α-$V_2O_5$, respectively. α-$V_2O_5$ is a non-protective oxide and $TiO_2$ is still not in enough amounts to form a continuous protective scale, reason why a linear oxidation rate is observed. For longer oxidation times, the progressive thickening of the Ti-rich oxide scale will make difficult the oxygen diffusion inward retarding the reaction and promoting the parabolic behaviour. However, the protection is not so efficient as in TiN and/or Ti-Si-N samples (see Figures 5) due to the disruption induced by the outward/lateral diffusion of V ions through the oxide scale. In any condition the protective Si-O layer could be also formed. Similar isothermal evolution was reported by Zhou et al. [36], which during isothermal oxidation of multilayered TiAlN/VN coatings have detected α-$V_2O_5$ at the initial stage of oxidation. In their system, the mass gain curves also showed initially a linear evolution, followed by a parabolic growth, similar to what was observed here for TiSiVN films. Keller and Douglass [45] also showed that pure vanadium oxidizes linearly, whereas the addition of different elements (Al, Cr, Ti) could transform the initial linear mass gain for a parabolic one due to the modification of the formed oxide layer.

At 700 $^0$C, temperature higher than the melting point of α-$V_2O_5$, very high oxidation rates were measured and high amounts of V-oxides were detected by XRD. The extremely high parabolic evolution suggests a very high diffusion rate of the reactive ions through the oxide scales.

A comparison between TiSiVN with CrAlVN and TiAlVN (in single layered or multilayered configuration) coatings, reveals a lower onset point of oxidation of approximately 100 $^0$C. In CrAlVN and TiAlVN coatings the onset point of oxidation was close to ~600 $^0$C [8, 36, 37]. In the case of the TiAlVN films, signals of lubricious α-$V_2O_5$ were detected as soon as the oxidation started, while at high temperatures only $AlVO_4$ and $TiO_2$ were identified [8]. For CrAlVN coatings, $AlVO_4$, (Al, Cr, V)$_2O_3$ as

well as α-$V_2O_5$ oxides were observed for an annealing temperature of 700 $^0$C [37]. In these studies, the lower onset point of oxidation displayed by the V-containing coatings was explained by the reactions occurring between protective oxides and vanadium (such as formation of Al-V-O phases). In the present TiSiVN system combination of V with titanium or silicon oxide was not detected. Therefore, we suggest that the loss of oxidation resistance of TiSiVN coatings is due to the rapid oxidation of V and the outwards diffusion of its ions through the Ti-rich oxide scale. Further work is needed to understand the mechanisms involved during the oxidation deterioration of TiSiN coatings with V additions and their corresponding oxide scale formation. The performance of solid solution coatings for high temperature sliding application should be investigated in further work. Rapid formation of vanadium oxide could indeed reduce friction at temperatures higher than 500 $^0$C; nonetheless, the wear resistance of the coating can be significantly compromised by low oxidation resistance. In future research, we propose to deposit nanocomposite structure of TiSiVN combining nanograins of c-TiVN embedded into amorphous Si-N matrix, to control the outwards diffusion of vanadium.

## 4. Conclusion

This investigation concerned the influence of V additions on the structure, mechanical properties and oxidation resistance of Ti-Si-V-N coatings deposited by DC reactive magnetron sputtering. These coatings were compared to TiN and TiSiN films. According to XRD analyses, all coatings showed an fcc NaCl-type structure assigned to crystalline TiN. A shift of the peaks to the right was observed with Si and V additions, indicative of a substitutional solid solution. Hardness and Young modulus of TiSiN

coatings was insignificantly changed with increasing V content. The onset of oxidation of the coatings decreased with V additions down to temperatures as low as 500 $^0$C, independently of the Si and V content in the coatings. TiN and TiSiN coating exhibits a typical parabolic oxidation weight gain as a function of time, while a different evolution is displayed by TiSiVN films. At temperatures below the melting point of α-$V_2O_5$ (~685 $^0$C) two stages were exhibited: at an early stage, the weight increase over time is linear, whilst, in a second stage a parabolic evolution could be fitted to the experimental data; on the other hand, at high temperatures only a parabolic evolution was fitted. α-$V_2O_5$ showed to be the main phase present at the oxidized surface of coatings. Reduction of this phase occurred for temperatures above their melting point. The relative amounts of $V_2O_5$ detected at the oxidized surface of V rich films are promising to achieve the envisaged good tribological properties; however it can be significantly compromised by their low oxidation resistance.

**Acknowledgments**

This research is sponsored by FEDER funds through the program COMPETE – Programa Operacional Factores de Competitividade – and by national funds through FCT – Fundação para a Ciência e a Tecnologia –, under the projects: PEst-C/EME/UI0285/2013, CENTRO-07-0224-FEDER-002001 (Mais Centro SCT_2011_02_001_4637), PTDC/EME-TME/122116/2010 and Plungetec, as well as the grant (SFRH/BD/68740/2010).

**References**

[1] Z. Zhou, W.M. Rainforth, D.B. Lewis, S. Creasy, J.J. Forsyth, F. Clegg, A.P. Ehiasarian, P.E. Hovespian, W.D. Münz, Oxidation behaviour of nanoscale TiAlN/VN multilayer coatings, Surf. Coat. Technol., 177–178 (2004) 198-203.

[2] M. Pfeiler, K. Kutschej, M. Penoy, C. Michotte, C. Mitterer, M. Kathrein, The effect of increasing V content on structure, mechanical and tribological properties of arc evaporated Ti–Al–V–N coatings, International Journal of Refractory Metals and Hard Materials, 27 (2009) 502-506.

[3] N. Fateh, G.A. Fontalvo, G. Gassner, C. Mitterer, Influence of high-temperature oxide formation on the tribological behaviour of TiN and VN coatings, Wear, 262 (2007) 1152-1158.

[4] E. Badisch, G.A. Fontalvo, M. Stoiber, C. Mitterer, Tribological behavior of PACVD TiN coatings in the temperature range up to 500 °C, Surf. Coat. Technol., 163–164 (2003) 585-590.

[5] M. Stoiber, E. Badisch, C. Lugmair, C. Mitterer, Low-friction TiN coatings deposited by PACVD, Surf. Coat. Technol., 163–164 (2003) 451-456.

[6] E. Lugscheider, O. Knotek, K. Bobzin, S. Bärwulf, Tribological properties, phase generation and high temperature phase stability of tungsten- and vanadium-oxides deposited by reactive MSIP-PVD process for innovative lubrication applications, Surf. Coat. Technol., 133–134 (2000) 362-368.

[7] D.B. Lewis, S. Creasey, Z. Zhou, J.J. Forsyth, A.P. Ehiasarian, P.E. Hovsepian, Q. Luo, W.M. Rainforth, W.D. Münz, The effect of (Ti+Al):V ratio on the structure and oxidation behaviour of TiAlN/VN nano-scale multilayer coatings, Surf. Coat. Technol., 177–178 (2004) 252-259.

[8] K. Kutschej, P.H. Mayrhofer, M. Kathrein, P. Polcik, C. Mitterer, Influence of oxide phase formation on the tribological behaviour of Ti–Al–V–N coatings, Surf. Coat. Technol., 200 (2005) 1731-1737.

[9] K. Kutschej, P.H. Mayrhofer, M. Kathrein, P. Polcik, C. Mitterer, A new low-friction concept for Ti1−xAlxN based coatings in high-temperature applications, Surf. Coat. Technol., 188–189 (2004) 358-363.

[10] G. Gassner, P.H. Mayrhofer, K. Kutschej, C. Mitterer, M. Kathrein, A New Low Friction Concept for High Temperatures: Lubricious Oxide Formation on Sputtered VN Coatings, Tribology Letters, 17 (2004) 751-756.

[11] P.H. Mayrhofer, P.E. Hovsepian, C. Mitterer, W.D. Münz, Calorimetric evidence for frictional self-adaptation of TiAlN/VN superlattice coatings, Surf. Coat. Technol., 177–178 (2004) 341-347.

[12] A. Glaser, S. Surnev, F.P. Netzer, N. Fateh, G.A. Fontalvo, C. Mitterer, Oxidation of vanadium nitride and titanium nitride coatings, Surface Science, 601 (2007) 1153-1159.

[13] M. Uchida, N. Nihira, A. Mitsuo, K. Toyoda, K. Kubota, T. Aizawa, Friction and wear properties of CrAlN and CrVN films deposited by cathodic arc ion plating method, Surf. Coat. Technol., 177–178 (2004) 627-630.

[14] J.H. Ouyang, S. Sasaki, Tribo-oxidation of cathodic arc ion-plated (V,Ti)N coatings sliding against a steel ball under both unlubricated and boundary-lubricated conditions, Surf. Coat. Technol., 187 (2004) 343-357.

[15] J.-K. Park, Y.-J. Baik, Increase of hardness and oxidation resistance of VN coating by nanoscale multilayered structurization with AlN, Mater. Lett., 62 (2008) 2528-2530.

[16] R. Franz, J. Neidhardt, R. Kaindl, B. Sartory, R. Tessadri, M. Lechthaler, P. Polcik, C. Mitterer, Influence of phase transition on the tribological performance of arc-evaporated AlCrVN hard coatings, Surf. Coat. Technol., 203 (2009) 1101-1105.

[17] Y. Qiu, S. Zhang, J.-W. Lee, B. Li, Y. Wang, D. Zhao, Self-lubricating CrAlN/VN multilayer coatings at room temperature, Applied Surface Science, 279 (2013) 189-196.

[18] W. Tillmann, S. Momeni, F. Hoffmann, A study of mechanical and tribological properties of self-lubricating TiAlVN coatings at elevated temperatures, Tribology International, 66 (2013) 324-329.

[19] Q. Luo, Temperature dependent friction and wear of magnetron sputtered coating TiAlN/VN, Wear, 271 (2011) 2058-2066.

[20] S.H. Kim, J.K. Kim, K.H. Kim, Influence of deposition conditions on the microstructure and mechanical properties of Ti–Si–N films by DC reactive magnetron sputtering, Thin Solid Films, 420–421 (2002) 360-365.

[21] M. Nose, Y. Deguchi, T. Mae, E. Honbo, T. Nagae, K. Nogi, Influence of sputtering conditions on the structure and properties of Ti–Si–N thin films prepared by r.f.-reactive sputtering, Surf. Coat. Technol., 174–175 (2003) 261-265.

[22] S. Veprek, H.D. Männling, P. Karvankova, J. Prochazka, The issue of the reproducibility of deposition of superhard nanocomposites with hardness of ≥50 GPa, Surf. Coat. Technol., 200 (2006) 3876-3885.

[23] D. Pilloud, J.F. Pierson, M.C. Marco de Lucas, A. Cavaleiro, Study of the structural changes induced by air oxidation in Ti–Si–N hard coatings, Surf. Coat. Technol., 202 (2008) 2413-2417.

[24] M. Diserens, J. Patscheider, F. Levy, Mechanical properties and oxidation resistance of nanocomposite TiN-SiNx physical-vapor-deposited thin films, Surface & Coatings Technology, 120 (1999) 158-165.

[25] F. Vaz, L. Rebouta, P. Goudeau, J. Pacaud, H. Garem, J.P. Rivière, A. Cavaleiro, E. Alves, Characterisation of Ti1−xSixNy nanocomposite films, Surf. Coat. Technol., 133–134 (2000) 307-313.

[26] M. Diserens, J. Patscheider, F. Lévy, Improving the properties of titanium nitride by incorporation of silicon, Surf. Coat. Technol., 108–109 (1998) 241-246.

[27] Y.H. Cheng, T. Browne, B. Heckerman, E.I. Meletis, Mechanical and tribological properties of nanocomposite TiSiN coatings, Surf. Coat. Technol., 204 (2010) 2123-2129.

[28] J. Patscheider, T. Zehnder, M. Diserens, Structure–performance relations in nanocomposite coatings, Surf. Coat. Technol., 146–147 (2001) 201-208.

[29] D. Ma, S. Ma, K. Xu, The tribological and structural characterization of nano-structured Ti–Si–N films coated by pulsed-d.c. plasma enhanced CVD, Vacuum, 79 (2005) 7-13.

[30] G. Stoney, The Tension of Metallic Films Deposited by Electrolysis, Proc. R. Soc, 82 (1909) 172-175.

[31] C.P. Constable, D.B. Lewis, J. Yarwood, W.D. Münz, Raman microscopic studies of residual and applied stress in PVD hard ceramic coatings and correlation with X-ray diffraction (XRD) measurements, Surf. Coat. Technol., 184 (2004) 291-297.

[32] F. Vaz, L. Rebouta, B. Almeida, P. Goudeau, J. Pacaud, J.P. Rivière, J. Bessa e Sousa, Structural analysis of Ti1−xSixNy nanocomposite films prepared by reactive magnetron sputtering, Surf. Coat. Technol., 120–121 (1999) 166-172.

[33] M. Diserens, J. Patscheider, F. Lévy, Mechanical properties and oxidation resistance of nanocomposite TiN–SiNx physical-vapor-deposited thin films, Surf. Coat. Technol., 120–121 (1999) 158-165.

[34] T. Kacsich, S. Gasser, Y. Tsuji, A. Dommann, M.A. Nicolet, A. Nicolet, Wet oxidation of Ti34Si23B43, Journal of Applied Physics, 85 (1999) 1871-1875.

[35] T. Kacsich, M.A. Nicolet, Moving species in Ti34Si23N43 oxidation, Thin Solid Films, 349 (1999) 1-3.

[36] Z. Zhou, W.M. Rainforth, C. Rodenburg, N.C. Hyatt, D.B. Lewis, P.E. Hovsepian, Oxidation Behavior and Mechanisms of TiAlN/VN Coatings, Metall. Mater. Trans. A, 38 (2007) 2464-2478.

[37] R. Franz, J. Neidhardt, C. Mitterer, B. Schaffer, H. Hutter, R. Kaindl, B. Sartory, R. Tessadri, M. Lechthaler, P. Polcik, Oxidation and diffusion processes during annealing of AlCrVN hard coatings, J. Vac. Sci. Technol. A, 26 (2008) 302-308.

[38] M. Wittmer, J. Noser, H. Melchior, Oxidation kinetics of TiN thin films, J Appl Phys, 52 (1981) 6659–6664.

[39] C.W. Zou, X.D. Yan, J. Han, R.Q. Chen, W. Gao, Microstructures and optical properties of β-V 2 O 5 nanorods prepared by magnetron sputtering, Journal of Physics D: Applied Physics, 42 (2009) 145402.

[40] A. Bouzidi, N. Benramdane, S. Bresson, C. Mathieu, R. Desfeux, M.E. Marssi, X-ray and Raman study of spray pyrolysed vanadium oxide thin films, Vibrational Spectroscopy, 57 (2011) 182-186.

[41] M. Fernández-García, X. Wang, C. Belver, J.C. Hanson, J.A. Rodriguez, Anatase-TiO2 Nanomaterials:  Morphological/Size Dependence of the Crystallization and Phase Behavior Phenomena, The Journal of Physical Chemistry C, 111 (2006) 674-682.

[42] R. J. Gonzales, Raman, *Infrared, X-ray, and EELS Studies of Nanophase Titania*, PhD dissertation, Virginia Polytechnic Institute, Blacksburg, Virginia, 1996, pp 426

[43] V.P. Filonenko, M. Sundberg, P.E. Werner, I.P. Zibrov, Structure of a high-pressure phase of vanadium pentoxide beta-V2O5, Acta Crystallographica Section B-Structural Science, 60 (2004) 375-381.

[44] P. Balog, D. Orosel, Z. Cancarevic, C. Schon, M. Jansen, V2O5 phase diagram revisited at high pressures and high temperatures, J. Alloys Compd., 429 (2007) 87-98.

[45] J.G. Keller, D.L. Douglass, The high-temperature oxidation behavior of vanadium-aluminum alloys, Oxid. Met., 36 (1991) 439-464.

**Figure Captions**

Figure 1 – XRD patterns of: a) TiSiN coatings with Si content ranging from 0 to 12.6 at.%. b) coating S1-0 with V additions.

Figure 2 - SEM fracture cross section micrographs of: a) coating TiN, b) coating S1-0, c) coating S1-12.

Figure 3 – a) Effect of Si content on hardness and Young's modulus for the TiN system. b) Effect of V content on hardness and Young's modulus for coating S1-0.

Figure 4 – Thermal gravimetric oxidation rate of coatings deposited on $Al_2O_3$ substrates using the linear-temperature ramp (RT to 1200 $^0$C at 20 $^0$C/min).

Figure 5 - Thermo gravimetric isothermal analysis of coatings exposed at different temperatures.

Figure 6 – X-ray diffraction patterns of oxidized surface of: coating S2-8 annealed at temperatures ranging 550 to 700 $^0$C.

Figure 7 – SEM observation of surface morphology of coating S2-0, after 1h oxidation at 900 $^0$C.

Figure 8 – Typical surface morphology of oxidized coatings: a) coating S2-8 exposed to 550 $^0$C during 1h, b) coating S2-8 exposed to 600 $^0$C during 10 min, c) coating S2-8 exposed to 600 $^0$C during 30 min, d) coating S2-8 exposed to 700 $^0$C during 10 min.

Figure 9 – Raman spectra of dark and light grey phases identified in Figure 7.

Figure 10 - Energy dispersive X-ray analysis (EDAX) of points 1 and 2 identified in Figure 8.

Figure 11 - Raman spectra of phase 1 and 2 identified in Figure 8.

Figure 12 - Raman spectra of phase 4 and 5 identified in Figure 8.

Fig 1 a)

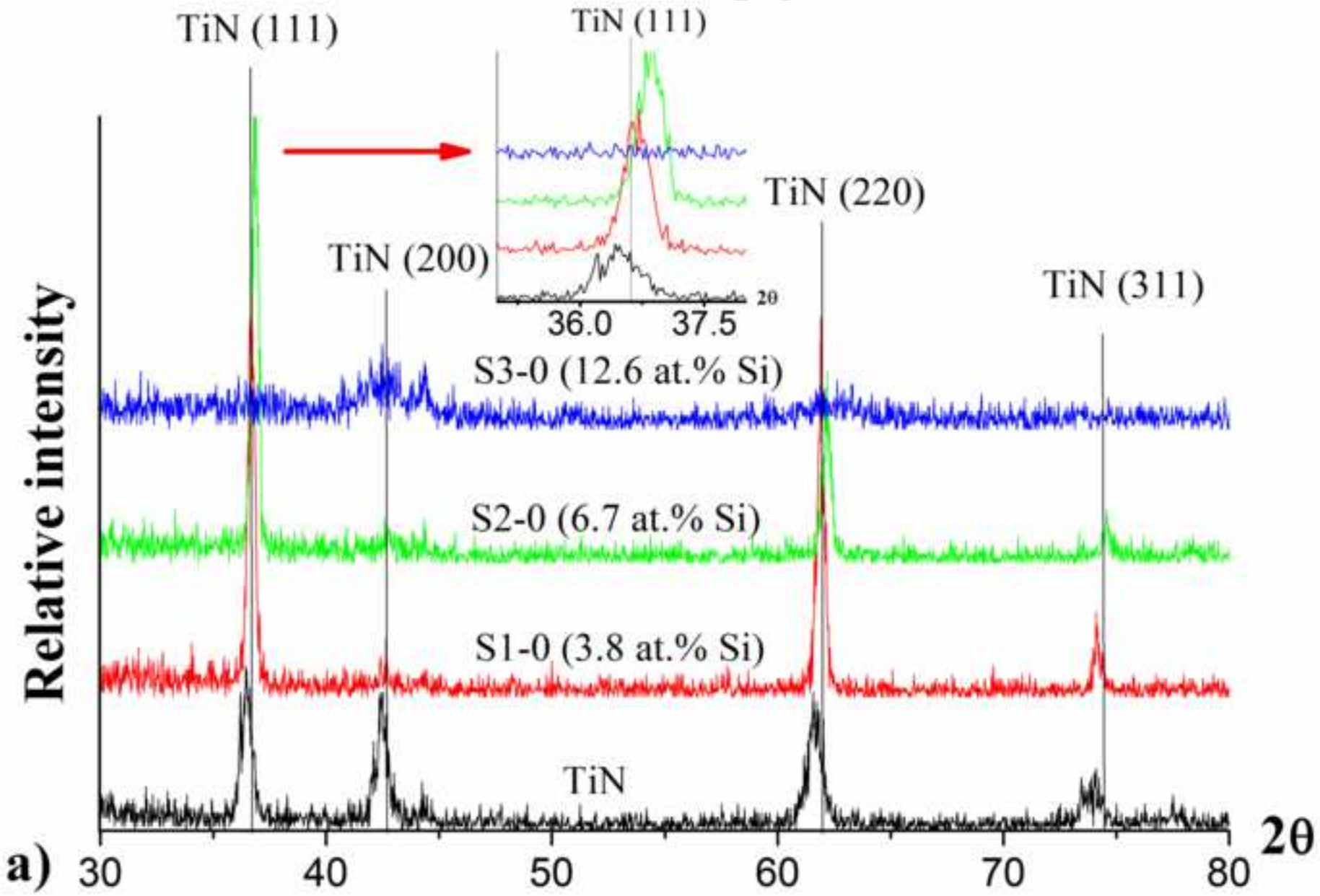
TiN (111)
TiN (111)
TiN (200)
TiN (220)
TiN (311)
36.0
37.5
2θ
S3-0 (12.6 at.% Si)
S2-0 (6.7 at.% Si)
S1-0 (3.8 at.% Si)
TiN
Relative intensity
a)
30
40
50
60
70
80
2θ

Fig 1 b)

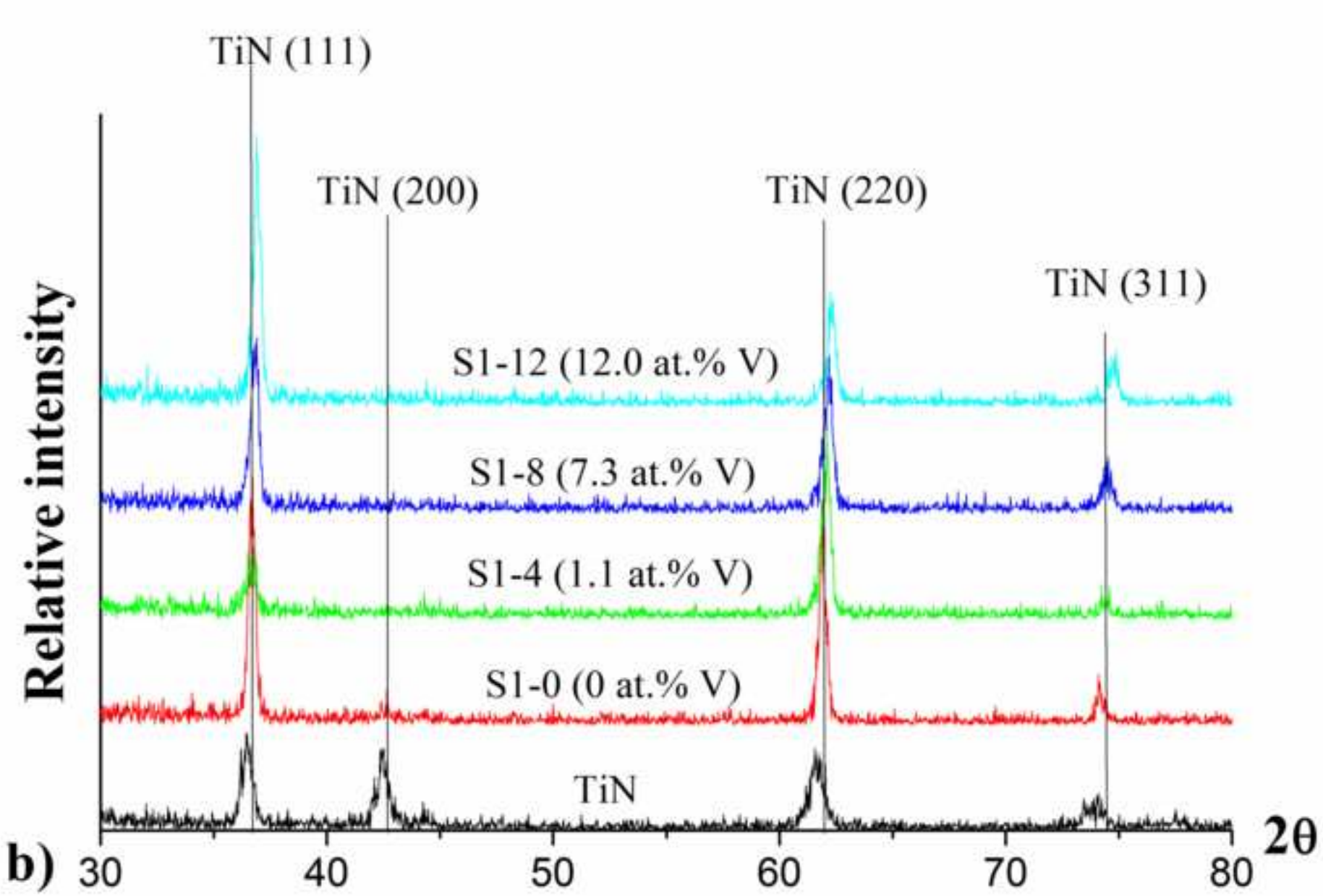
TiN (111)
TiN (200)
TiN (220)
TiN (311)
S1-12 (12.0 at.% V)
S1-8 (7.3 at.% V)
S1-4 (1.1 at.% V)
S1-0 (0 at.% V)
TiN
Relative intensity
b)
30
40
50
60
70
80
2θ

Fig 2 a)

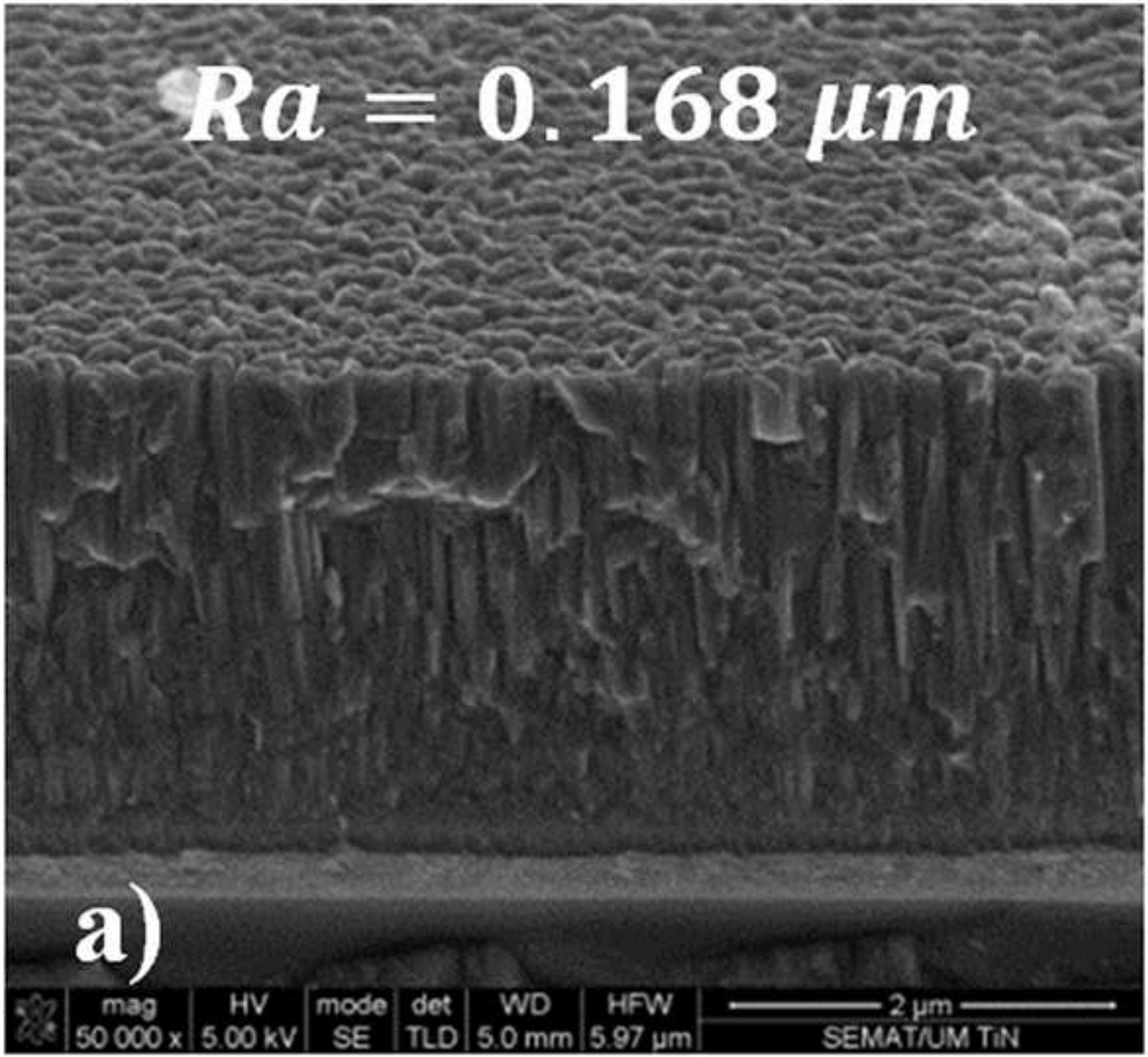
Ra = 0.168 µm
a)
mag
50 000 x
HV
5.00 kV
mode
SE
det
TLD
WD
5.0 mm
HFW
5.97 µm
2 µm
SEMATUM TiN

Fig 2 b)

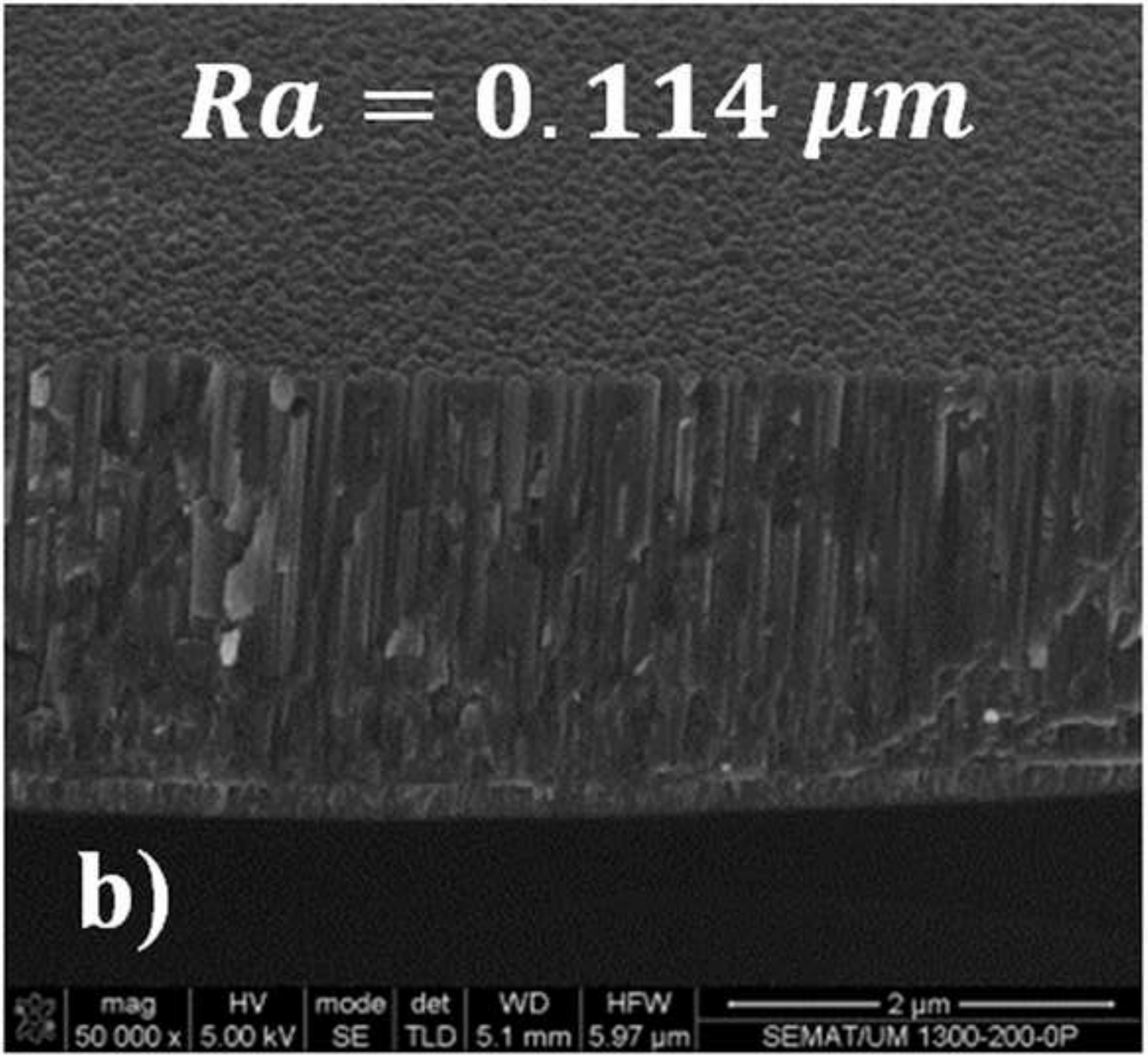
Ra = 0.114 µm
b)
mag
50 000 x
HV
5.00 kV
mode
SE
det
TLD
WD
5.1 mm
HFW
5.97 µm
2 µm
SEMAT/UM 1300-200-0P

Fig 2 c)

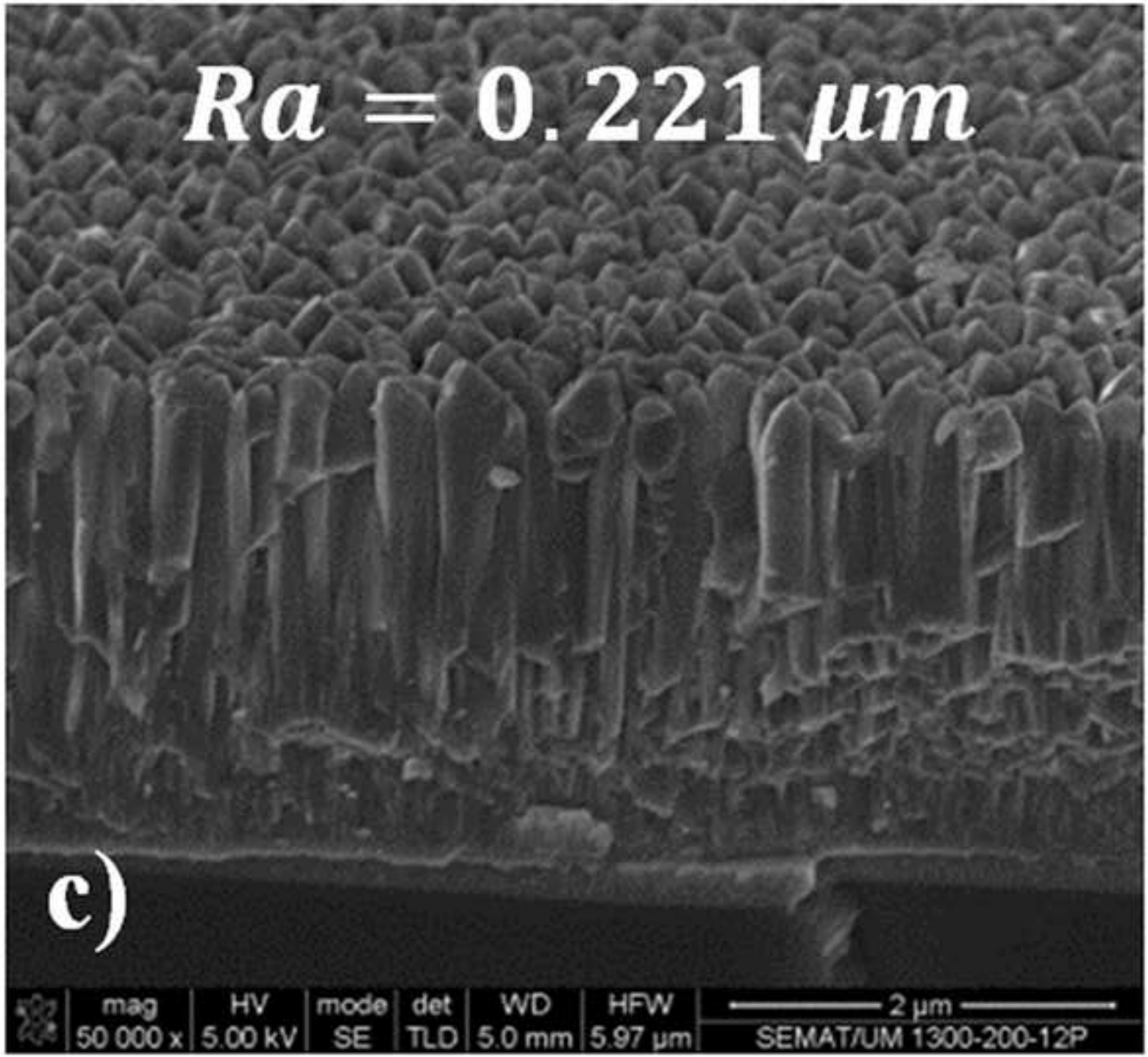
Ra = 0.221 µm
c)
mag
50 000 x
HV
5.00 kV
mode
SE
det
TLD
WD
5.0 mm
HFW
5.97 µm
2 µm
SEMAT/UM 1300-200-12P

Fig 3 a)

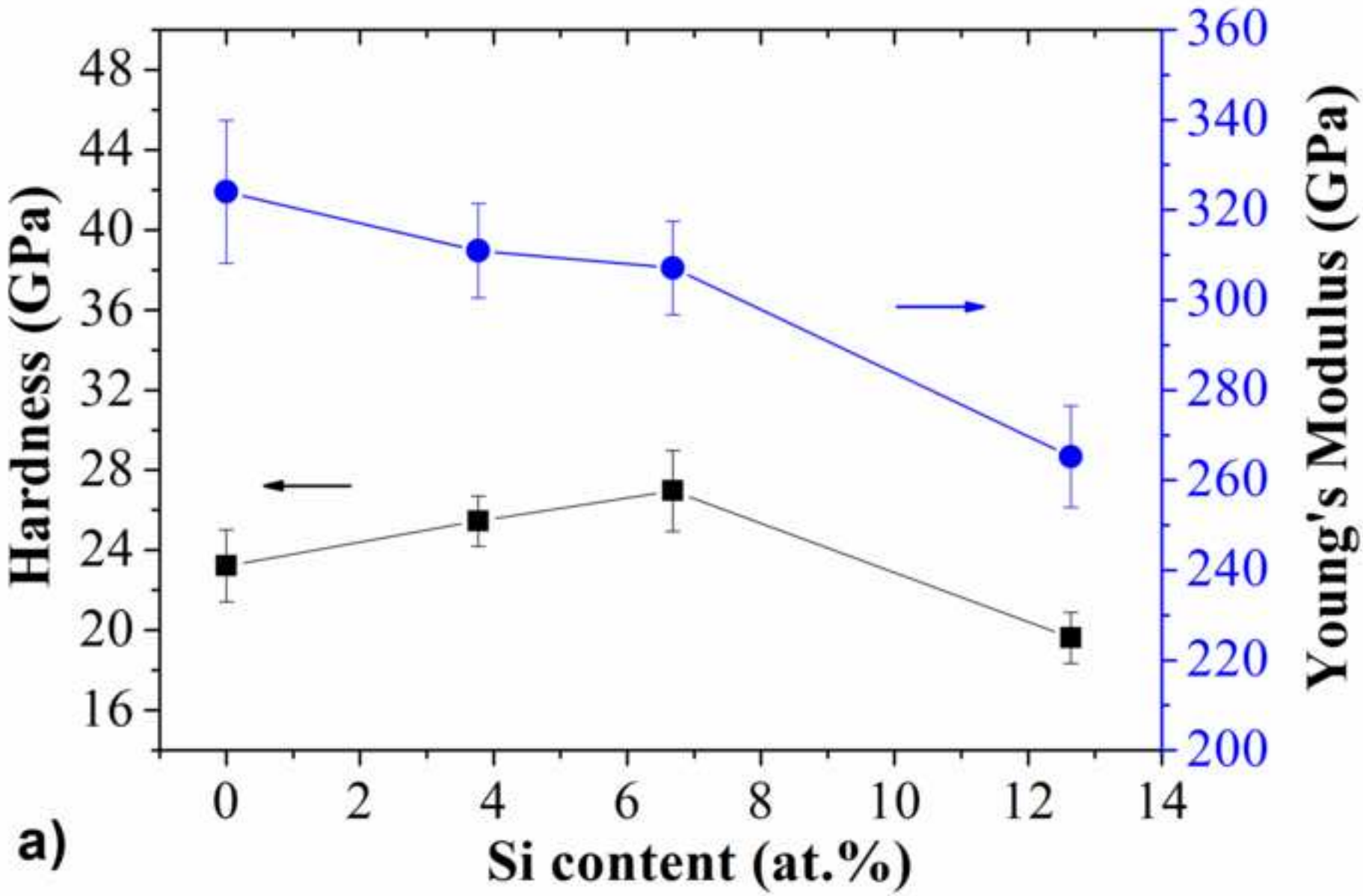
Hardness (GPa)
Young's Modulus (GPa)
Si content (at.%)
a)
48
44
40
36
32
28
24
20
16
360
340
320
300
280
260
240
220
200
0
2
4
6
8
10
12
14

Fig 3 b)

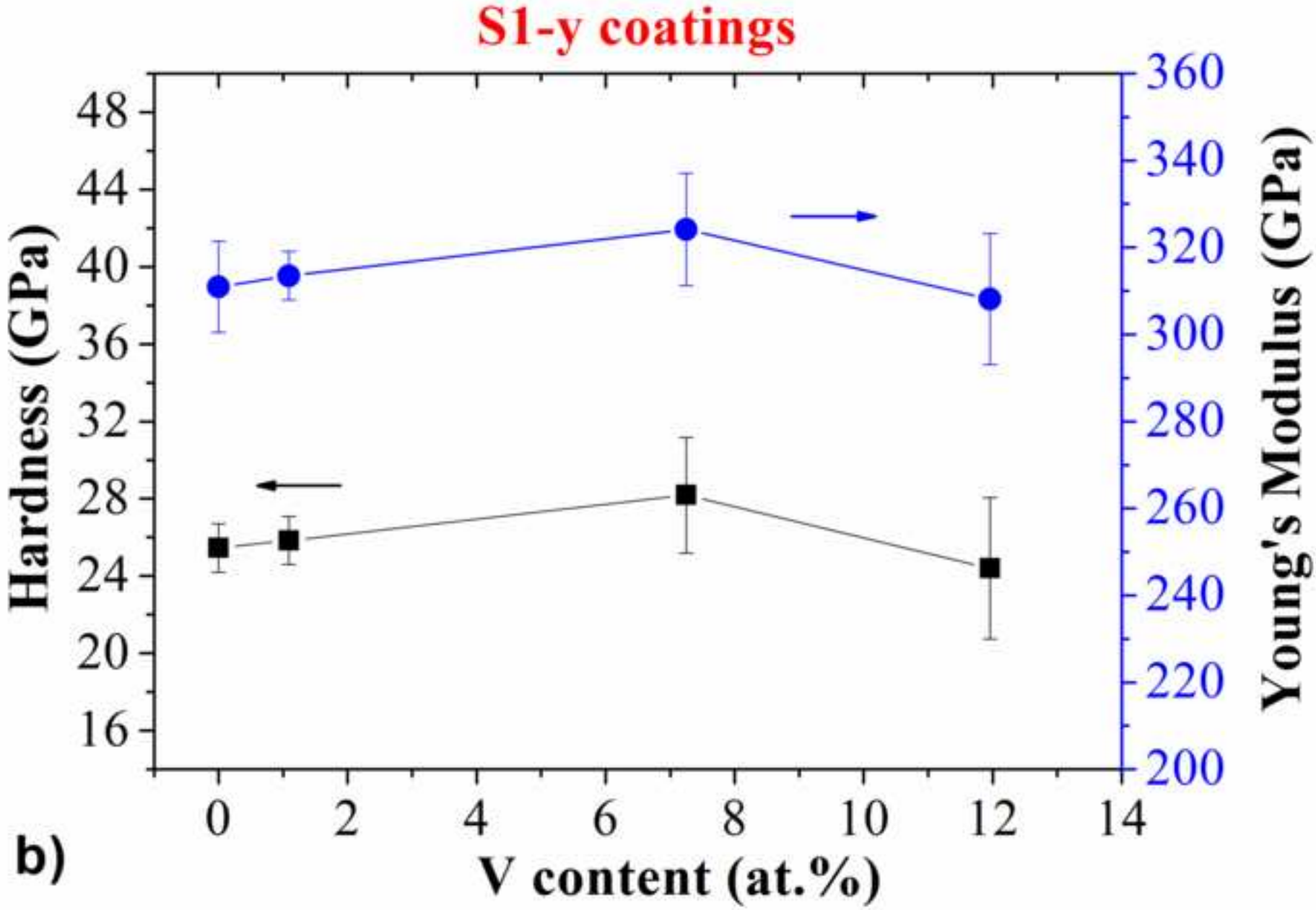
S1-y coatings
Hardness (GPa)
Young's Modulus (GPa)
V content (at.%)
48
44
40
36
32
28
24
20
16
360
340
320
300
280
260
240
220
200
0
2
4
6
8
10
12
14

b)

Fig 4

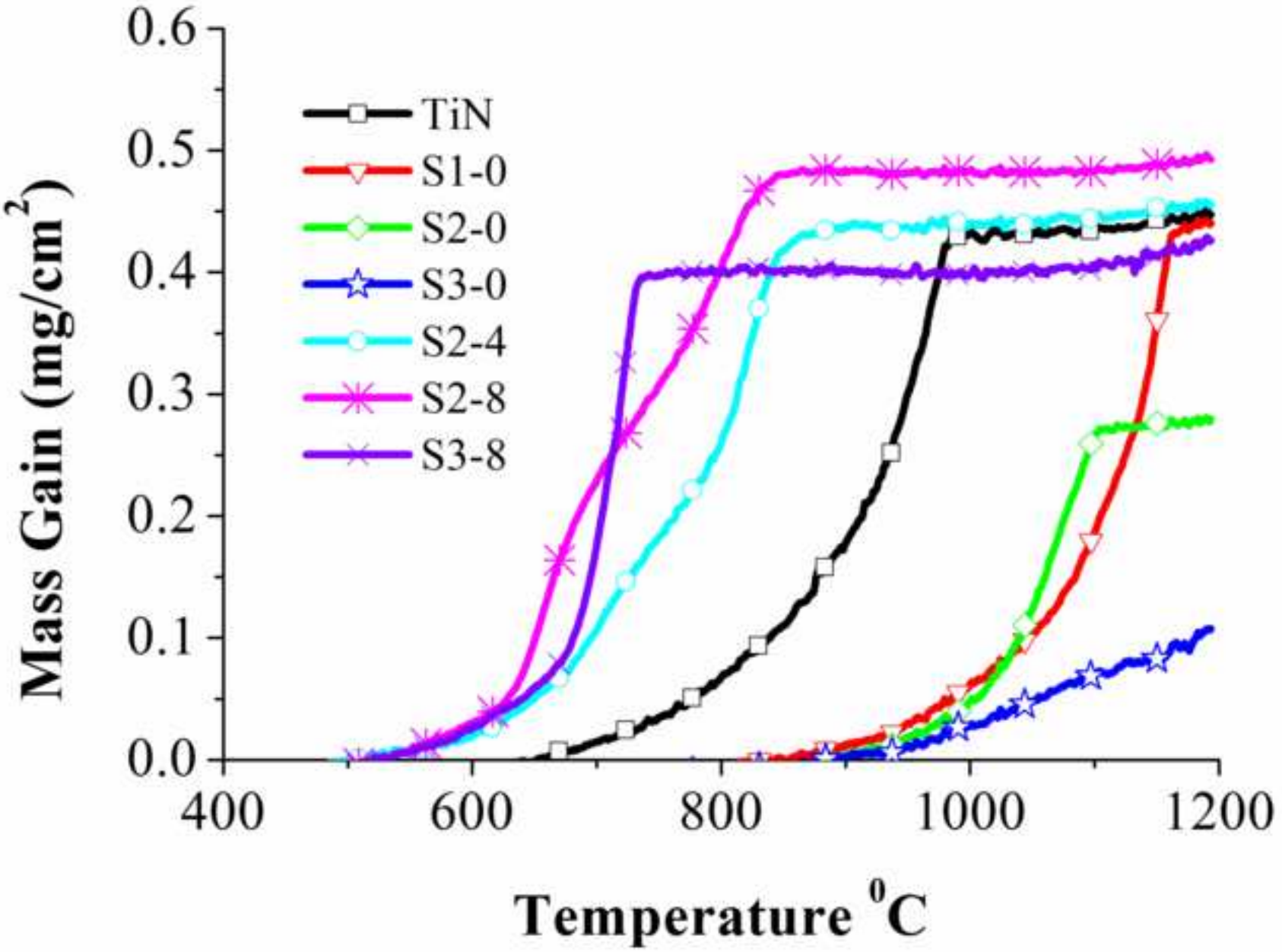
Mass Gain (mg/cm$^2$)
0.0
0.1
0.2
0.3
0.4
0.5
0.6
400
600
800
1000
1200
Temperature $^0$C
TiN
S1-0
S2-0
S3-0
S2-4
S2-8
S3-8

Fig 5

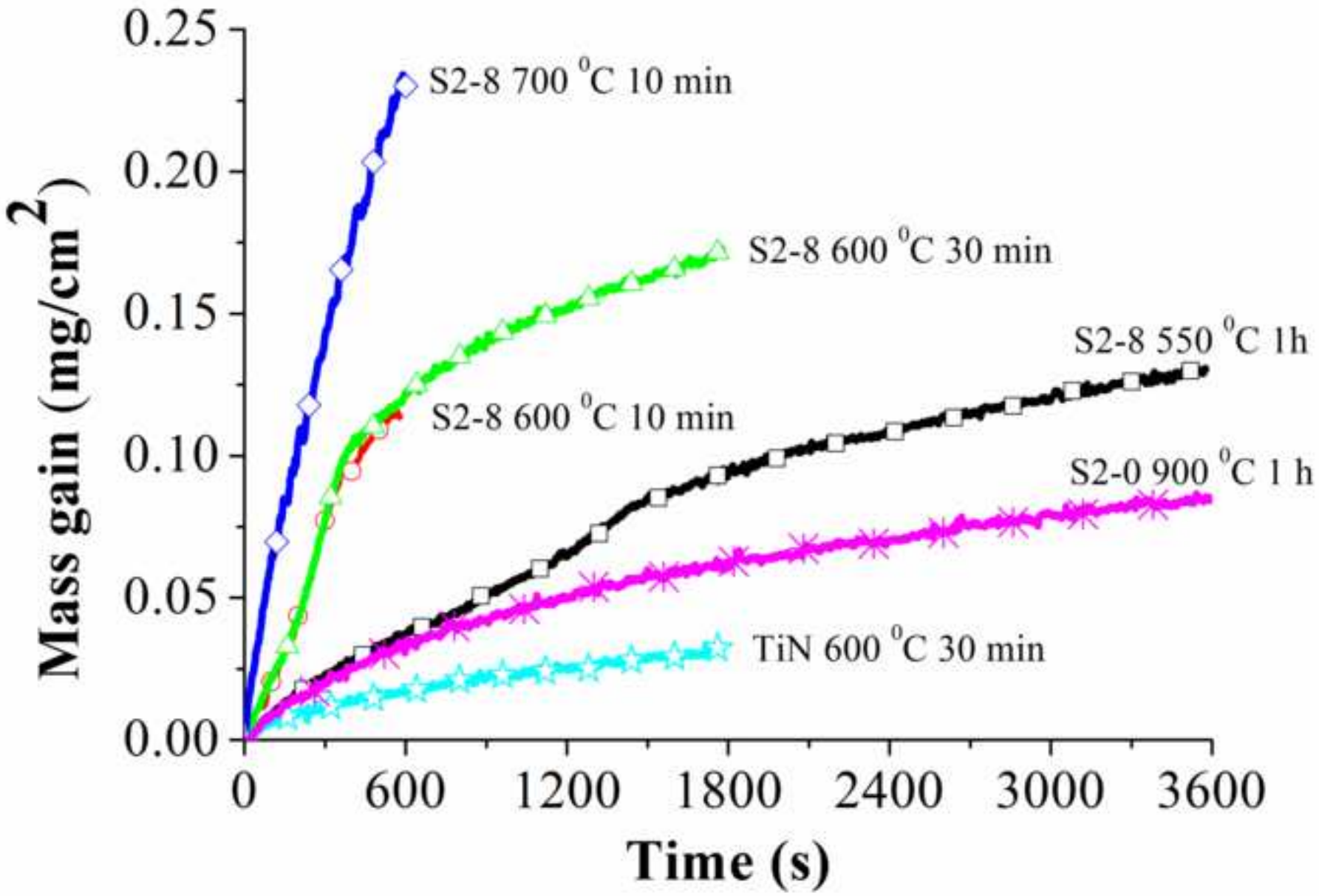
0.25
0.20
0.15
0.10
0.05
0.00
Mass gain (mg/cm$^2$)
0
600
1200
1800
2400
3000
3600
Time (s)
S2-8 700 $^0$C 10 min
S2-8 600 $^0$C 30 min
S2-8 550 $^0$C 1h
S2-8 600 $^0$C 10 min
S2-0 900 $^0$C 1 h
TiN 600 $^0$C 30 min

Fig 6

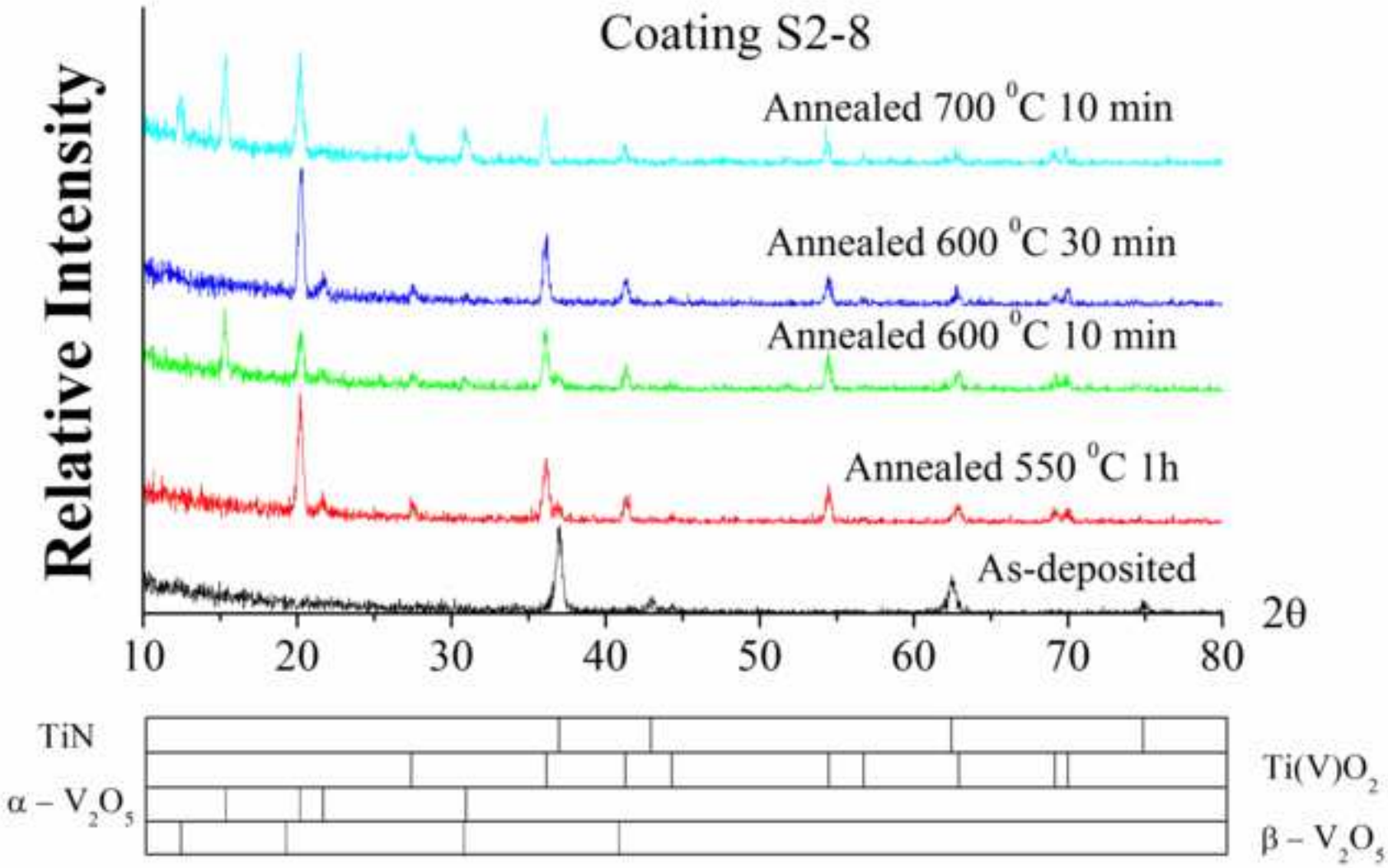
Coating S2-8
Relative Intensity
Annealed 700 °C 10 min
Annealed 600 °C 30 min
Annealed 600 °C 10 min
Annealed 550 °C 1h
As-deposited
2θ
10
20
30
40
50
60
70
80
TiN
α – V2O5
Ti(V)O2
β – V2O5

Fig 7

# S2-0 900 $^{0}$C 1h

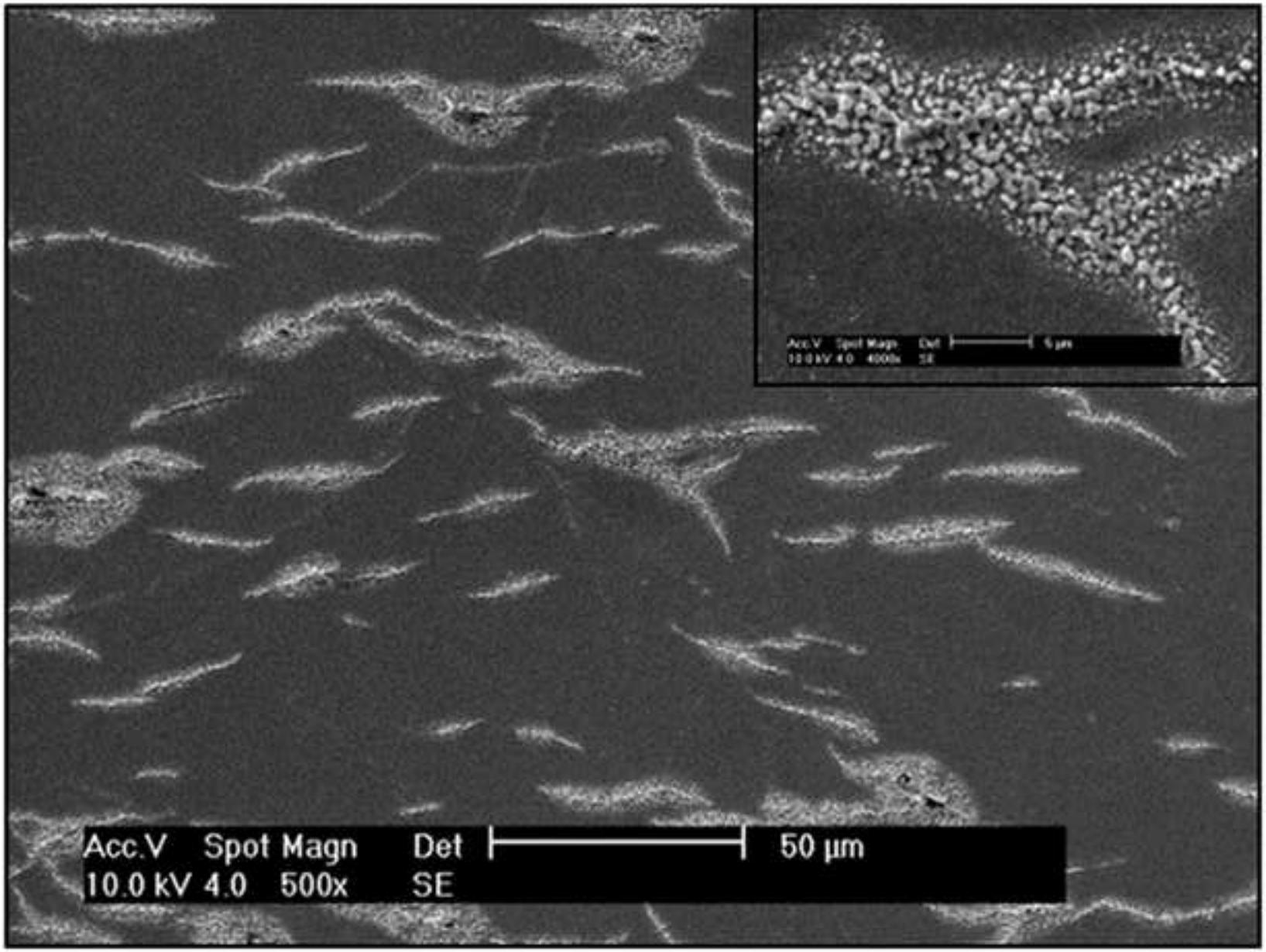

Fig 8

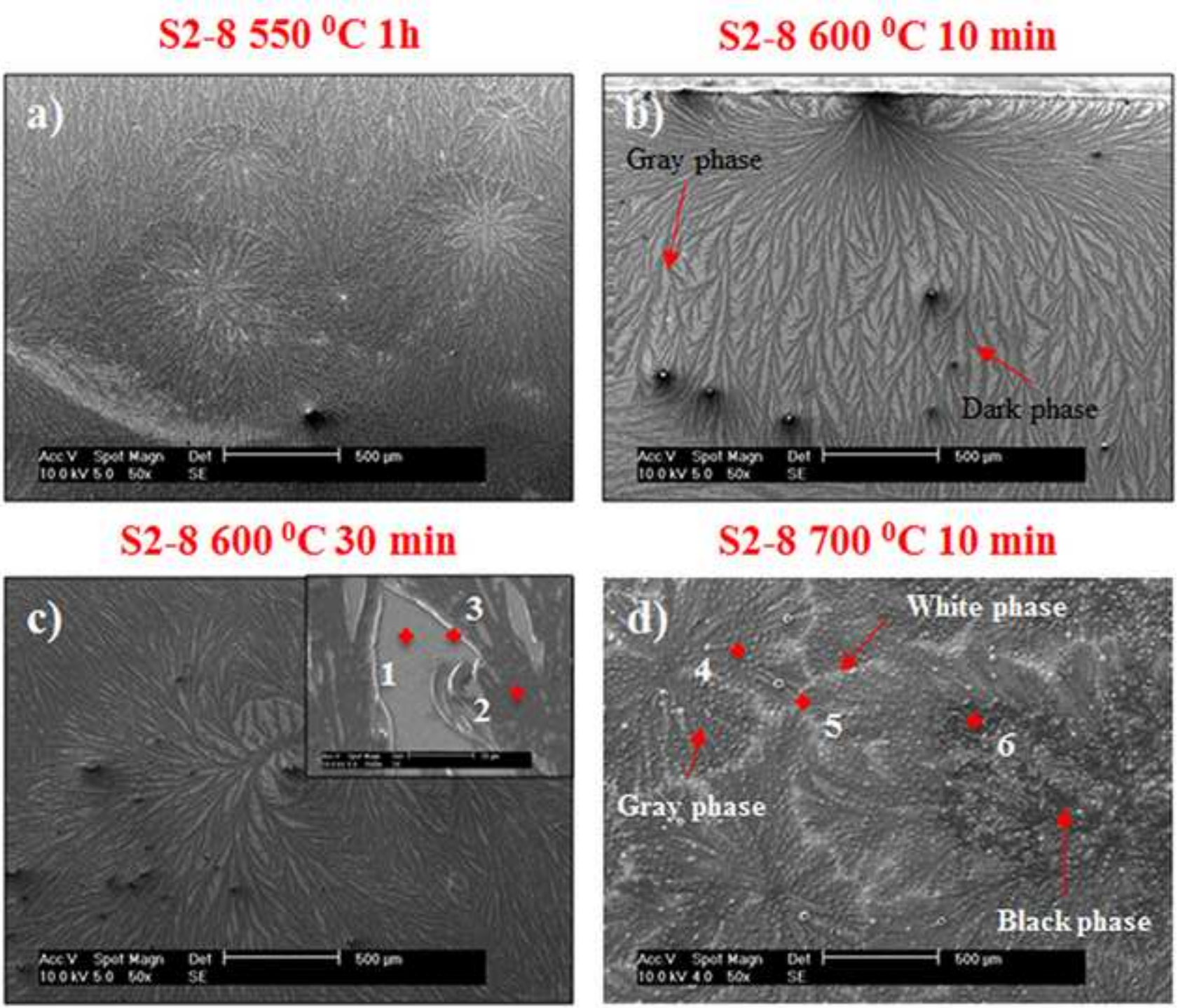
S2-8 550 $^0$C 1h
a)
Acc.V Spot Magn Det
10.0 kV 5.0 50x SE
500 µm
S2-8 600 $^0$C 10 min
b)
Gray phase
Dark phase
Acc.V Spot Magn Det
10.0 kV 5.0 50x SE
500 µm
S2-8 600 $^0$C 30 min
c)
1
2
3
Acc.V Spot Magn Det
10.0 kV 5.0 50x SE
500 µm
S2-8 700 $^0$C 10 min
d)
White phase
4
5
6
Gray phase
Black phase
Acc.V Spot Magn Det
10.0 kV 4.0 50x SE
500 µm

Fig 9

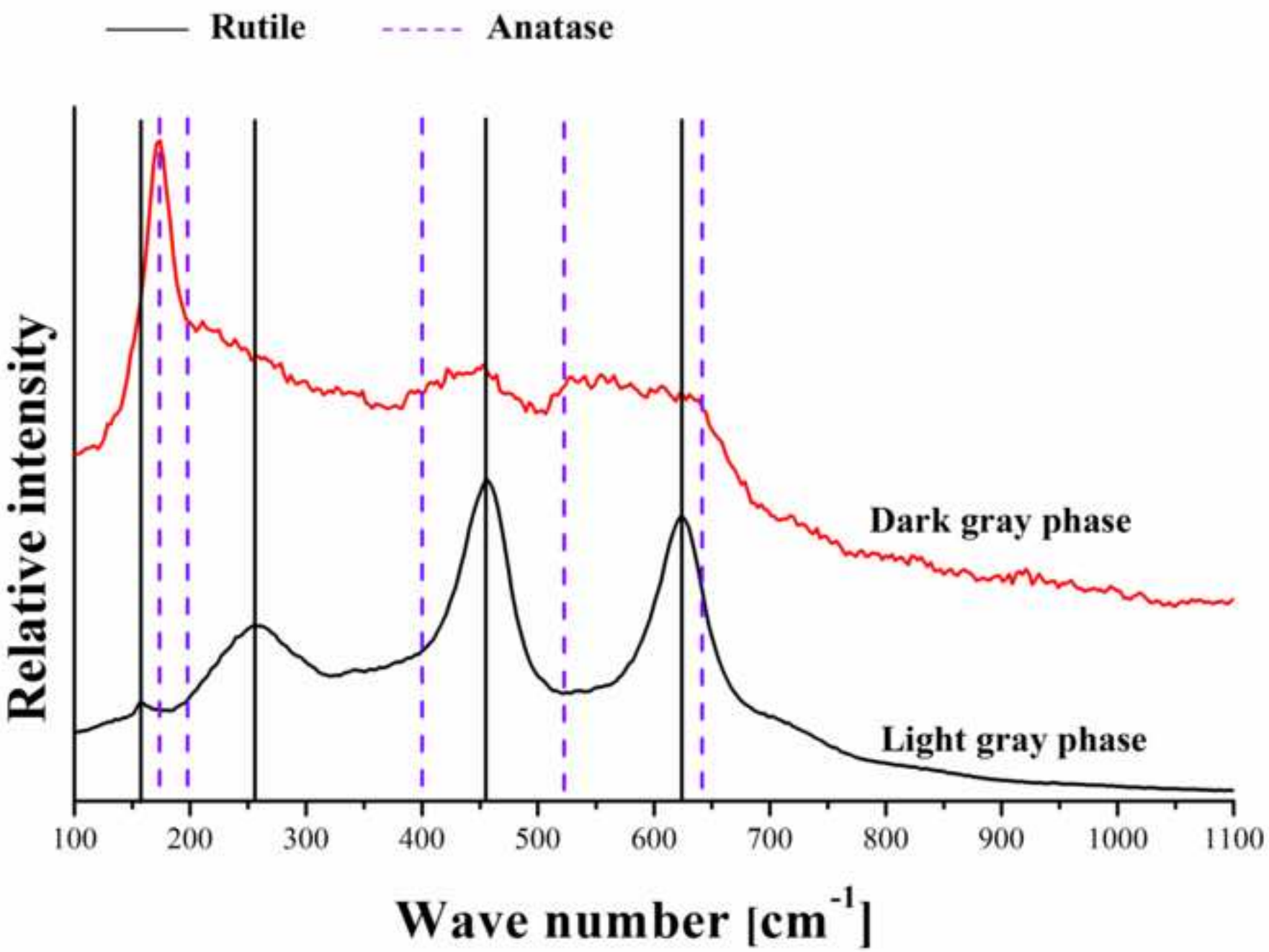
Rutile
Anatase
Relative intensity
Dark gray phase
Light gray phase
100
200
300
400
500
600
700
800
900
1000
1100
Wave number [cm-1]

Fig 10 a)

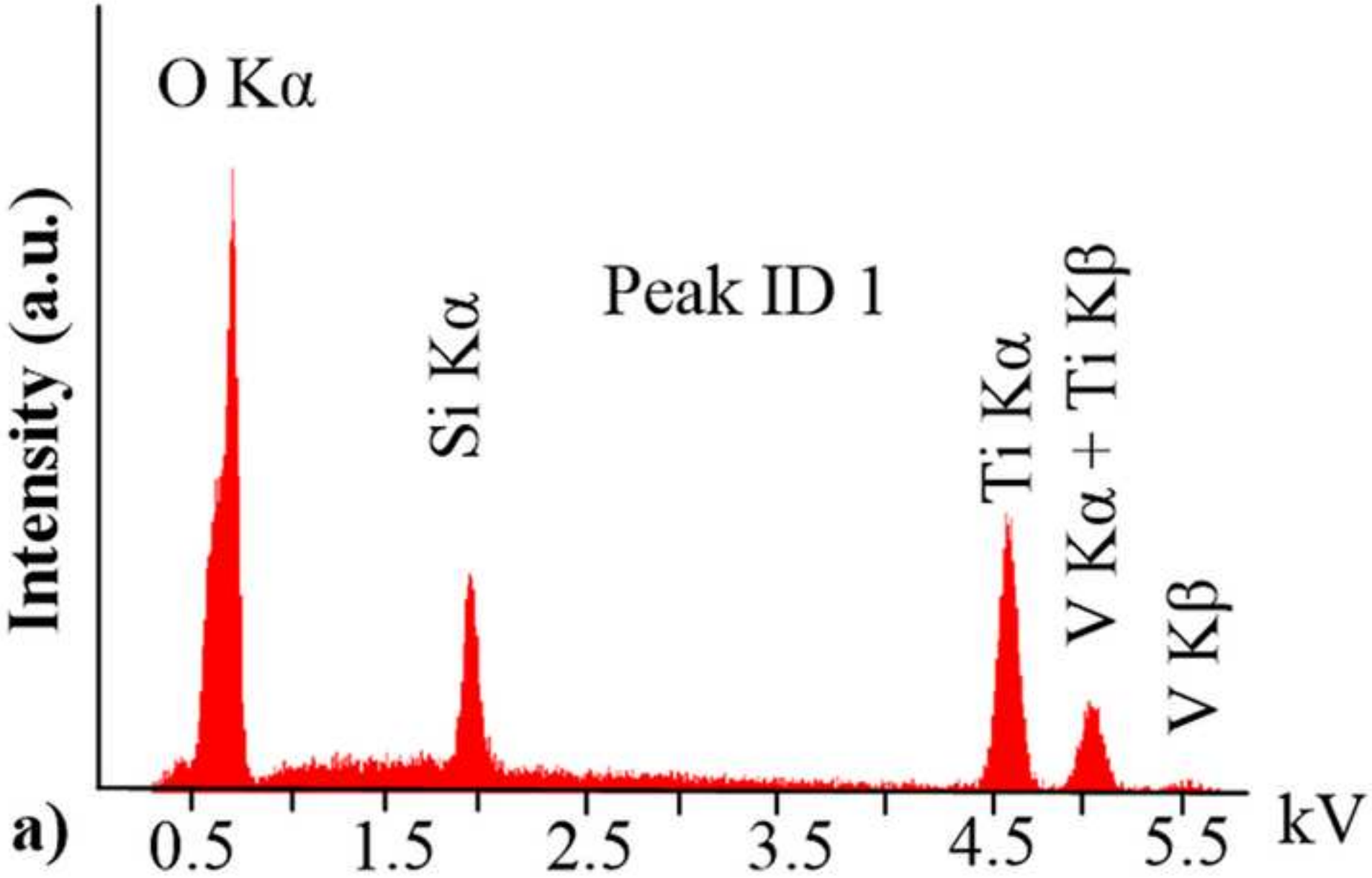
O Kα
Si Kα
Peak ID 1
Ti Kα
V Kα + Ti Kβ
V Kβ
Intensity (a.u.)
a)
0.5
1.5
2.5
3.5
4.5
5.5
kV

Fig 10 b)

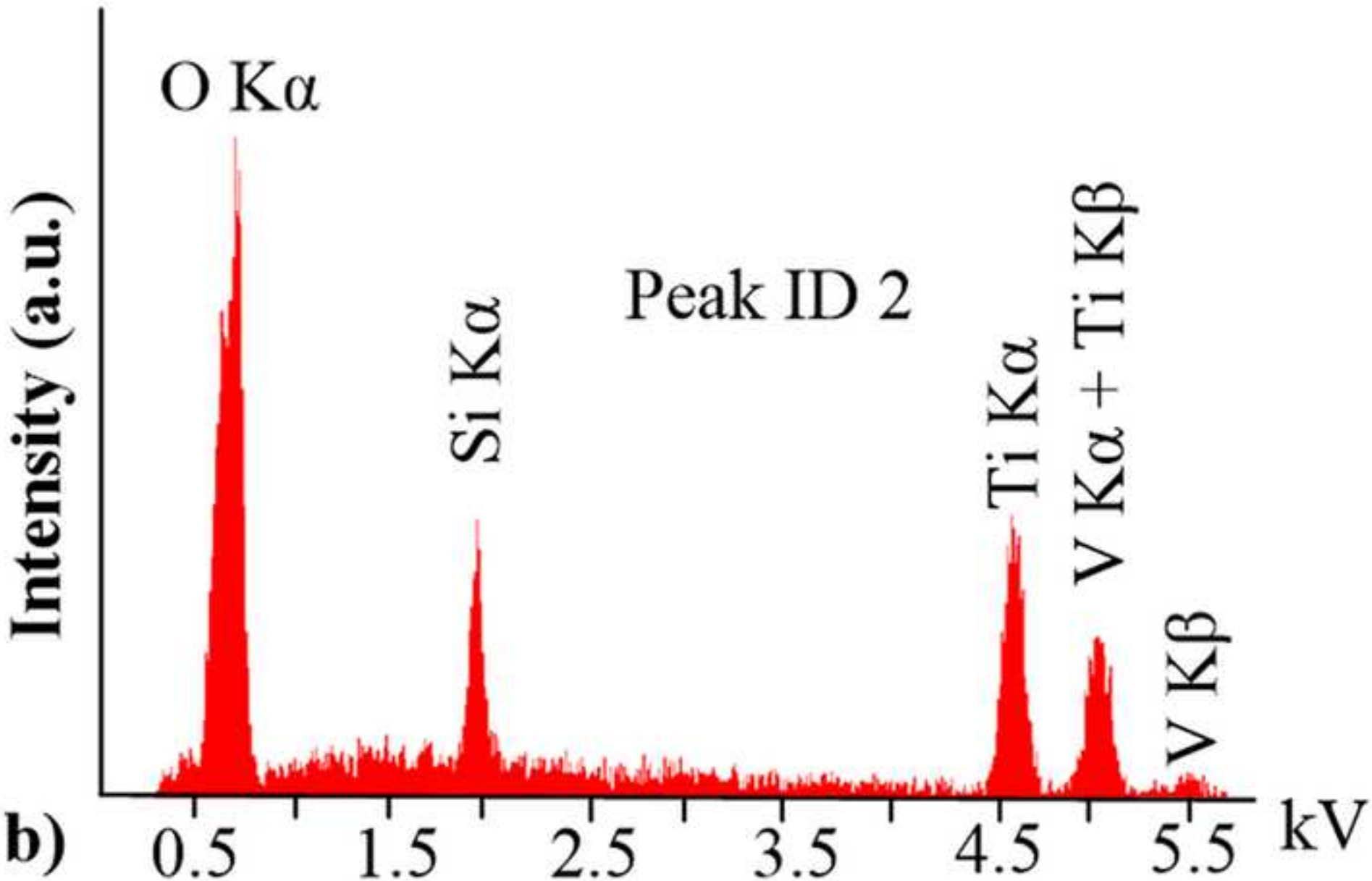
O Kα
Si Kα
Peak ID 2
Ti Kα
V Kα + Ti Kβ
V Kβ
Intensity (a.u.)
b)
0.5
1.5
2.5
3.5
4.5
5.5
kV

Fig 11

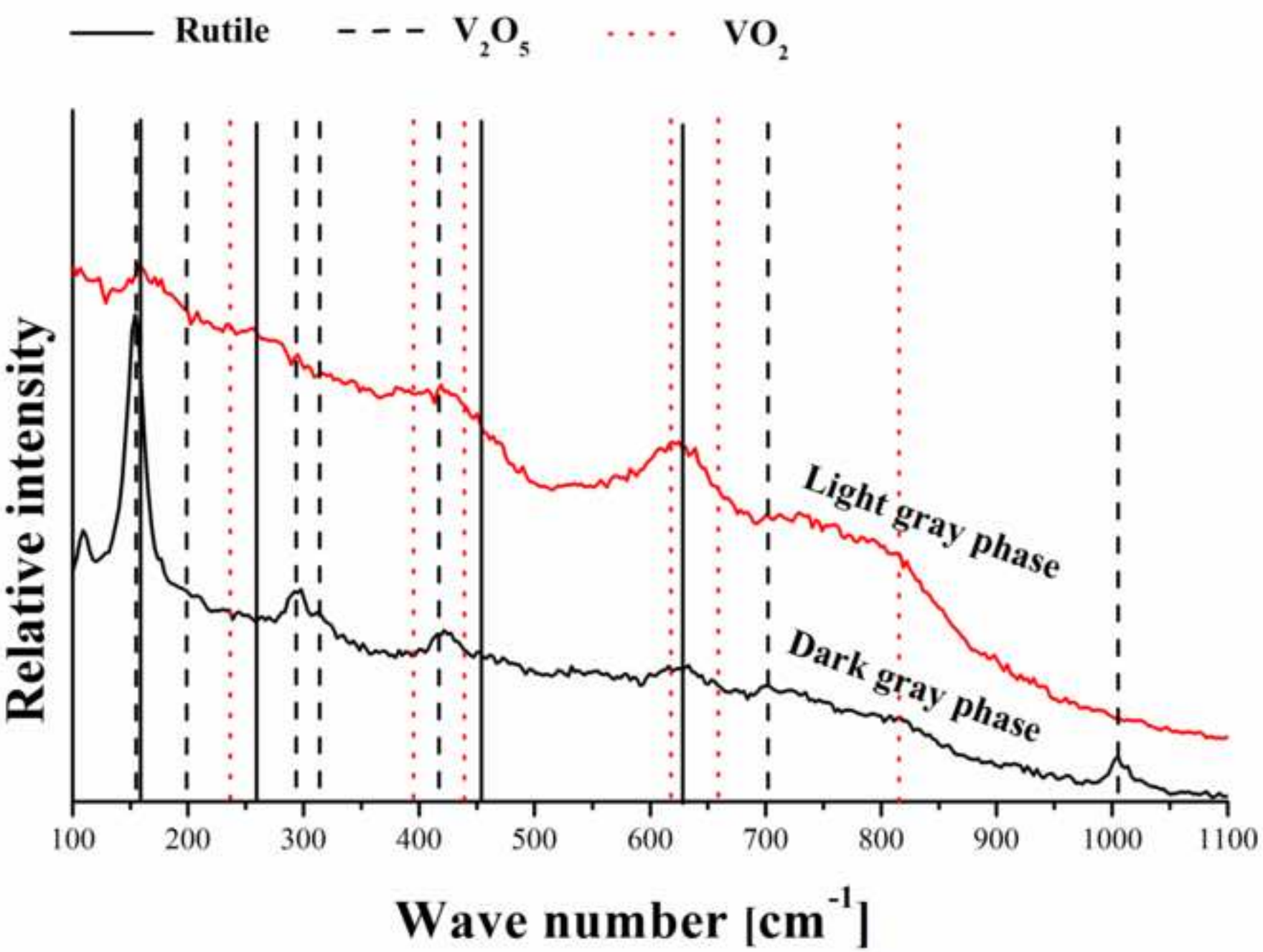
Rutile
V2O5
VO2
Relative intensity
Light gray phase
Dark gray phase
100
200
300
400
500
600
700
800
900
1000
1100
Wave number [cm-1]

Fig 12

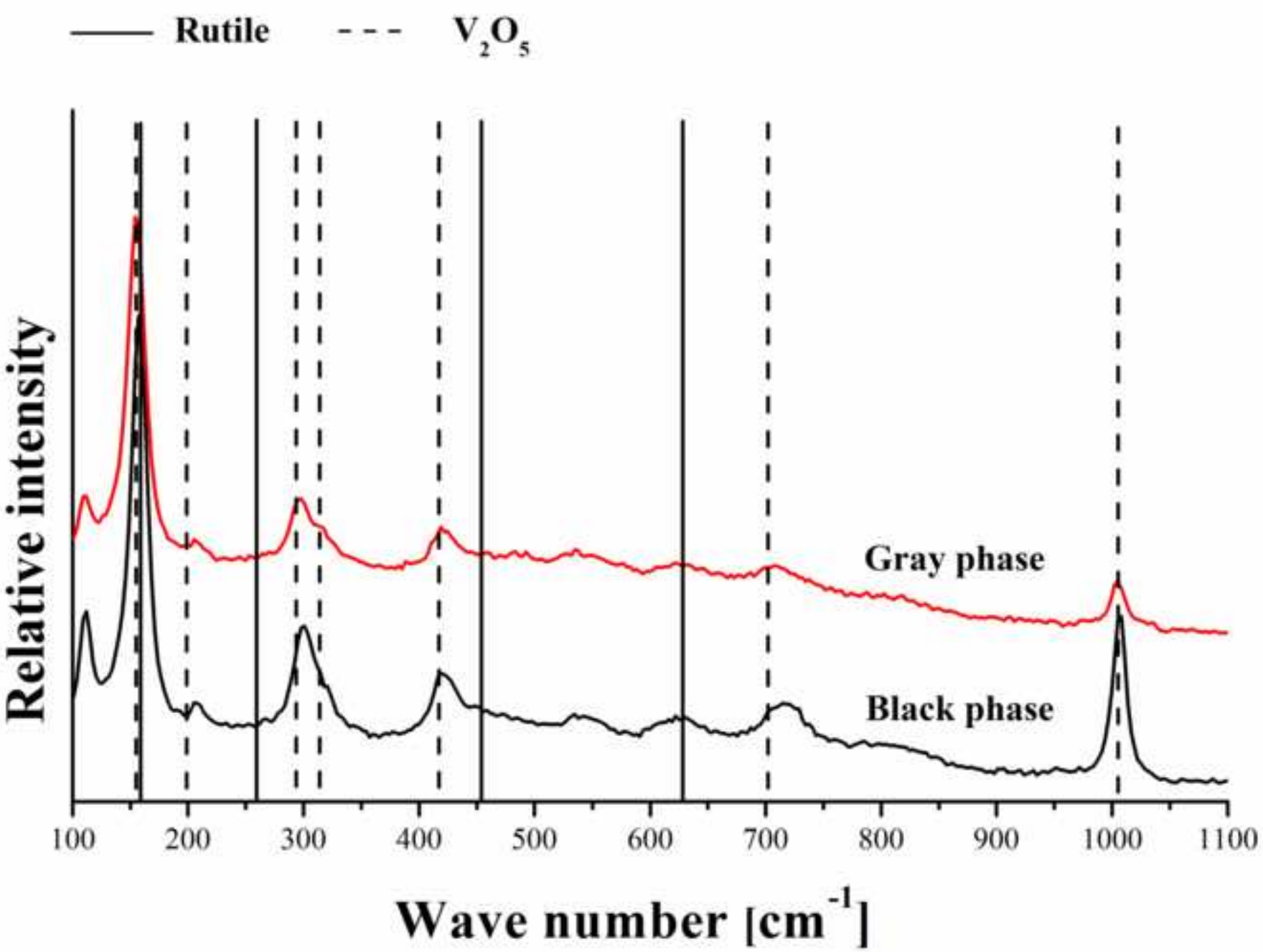
Rutile
V2O5
Relative intensity
Gray phase
Black phase
100
200
300
400
500
600
700
800
900
1000
1100
Wave number [cm-1]

Table 1 – Sample designation and deposition parameters of the coatings.

| | Sample | Target power density ($W/cm^2$) | | Deposition time (min) | Pellets of V at the Ti target |
|---|---|---|---|---|---|
| | | Ti | $TiSi_2$ | | |
| | Interlayer Ti | 10 | - | 5 | - |
| | Interlayer TiN | | - | 15 | - |
| TiSiN | S1-0 | 6.5 | 1 | 210 | 0 |
| TiSiVN | S1-4 | | | | 4 |
| | S1-8 | | | | 8 |
| | S1-12 | | | | 12 |
| TiSiN | S2-0 | 6 | 1.5 | 193 | 0 |
| TiSiVN | S2-4 | | | | 4 |
| | S2-8 | | | | 8 |
| | S2-12 | | | | 12 |
| TiSiN | S3-0 | 5 | 2.5 | 153 | 0 |
| TiSiVN | S3-4 | | | | 4 |
| | S3-8 | | | | 8 |
| | S3-12 | | | | 12 |
| | TiN | 10 | - | 73 | - |

Table 2 – Chemical composition of the dissimilar coatings in at.%.

| | | At.% | | | | |
|---|---|---|---|---|---|---|
| | Coating | N | O | Si | Ti | V |
| | TiN | 49.8 ± 0.1 | 0.4 ± 0.1 | - | 49.6 ± 0.4 | - |
| TiSiN | S1-0 | 51.1 ± 0.6 | 0.4 ± 0.1 | 3.8 ± 0.0 | 44.7 ± 0.7 | - |
| TiSiVN | S1-4 | 51.4 ± 0.4 | 1.5 ± 0.3 | 3.1 ± 0.0 | 43.0 ± 0.7 | 1.1 ± 0.1 |
| | S1-8 | 51.5 ± 0.2 | 1.2 ± 0.1 | 2.9 ± 0.0 | 37.1 ± 0.3 | 7.3 ± 0.1 |
| | S1-12 | 49.7 ± 0.3 | 1.8 ± 0.1 | 2.8 ± 0.0 | 33.8 ± 0.3 | 12.0 ± 0.1 |
| TiSiN | S2-0 | 51.5 ± 0.2 | 0.6 ± 0.1 | 6.7 ± 0.0 | 41.3 ± 0.3 | - |
| TiSiVN | S2-4 | 52.1 ± 0.2 | 1.2 ± 0.1 | 5.7 ± 0.0 | 39.3 ± 0.4 | 1.6 ± 0.2 |
| | S2-8 | 51.7 ± 0.1 | 1.4 ± 0.1 | 5.6 ± 0.1 | 33.6 ± 0.3 | 7.6 ± 0.2 |
| | S2-12 | 51.1 ± 0.6 | 1.9 ± 0.2 | 5.3 ± 0.0 | 30.5 ± 0.6 | 11.3 ± 0.1 |
| TiSiN | S3-0 | 51.4 ± 0.4 | 1.8 ± 0.1 | 12.6 ± 0.1 | 34.2 ± 0.5 | - |
| TiSiVN | S3-4 | 52.9 ± 0.1 | 1.5 ± 0.1 | 10.7 ± 0.0 | 32.1 ± 0.2 | 2.7 ± 0.1 |
| | S3-8 | 52.8 ± 0.2 | 2.0 ± 0.1 | 10.7 ± 0.1 | 27.2 ± 0.2 | 7.3 ± 0.1 |
| | S3-12 | 52.4 ± 0.3 | 2.1 ± 0.2 | 10.3 ± 0,1 | 24.9 ± 0.9 | 10.4 ± 0.1 |

Table 3 - Ratio between the peaks intensities of V Kβ (Si Kα) and Ti Kα from EDS analyses of points marked in Figure 8.

| | | Points | | | | | |
|---|---|---|---|---|---|---|---|
| | | 1 | 2 | 3 | 4 | 5 | 6 |
| Ratios | V Kβ/Ti Kα | 0.04 | 0.1 | 0.15 | 0.63 | 0.01 | 0.68 |
| | Si Kα/Ti Kα | 0.77 | 0.99 | 0.19 | 0.58 | 0.49 | 1.00 |